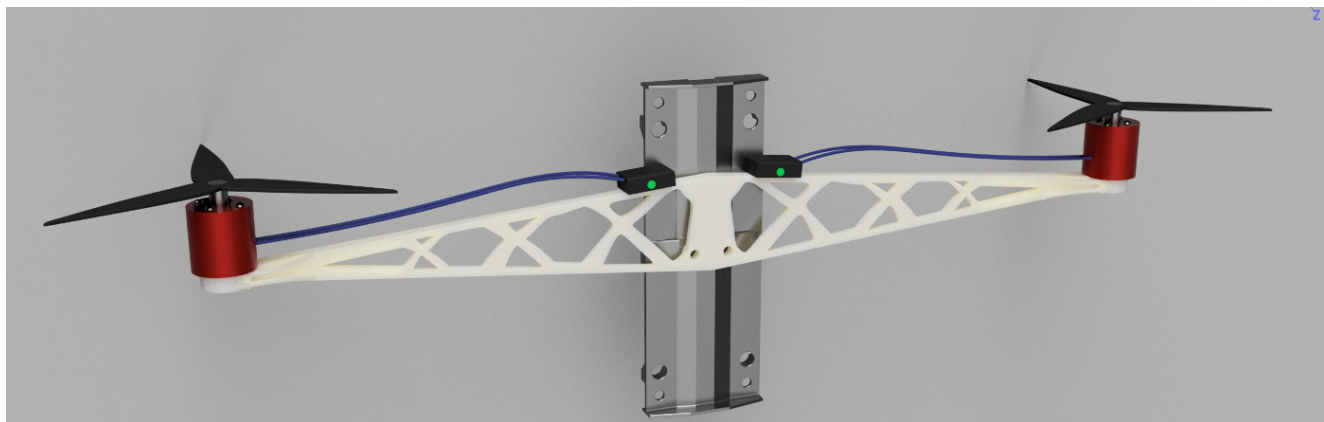


Design and Optimisation of a Structural Member and Control Law for a 1-DoF Duo-Copter.



Engineering Practice 2 - Technical - Group 11

Arush Bhattacharyya	02387477
Enoch Wong	02058833
Himmat Kaul	02376386
Jayden Jackson	02223479
Merrick Guo	02198840
Shankarshan Kundu	02224871

Date: June 2, 2025

Abstract

The following report outlines the methodology and procedures in the design, processing and manufacturing of a single degree-of-freedom (DOF) duocopter. There were two overarching problems to confront; the design of the two arms and a control law to handle throttle input. Linking both problems was a common objective to: maximise tracking accuracy of the controller, minimise power consumption and minimise manufacturing costs. Through a combination of heuristic parameter sweeps and SIMP topology optimisation in Abaqus, two structural members of total mass 52.58 g, tip deflection of 2.82 mm, stress safety factor of 4.1 and buckling safety factor of 2.64. A final total print cost of \$12.74 was achieved. Control design centred around development of a dynamic model, choosing and tuning a PID controller to minimise tracking error, quantified by a final RMSE of 0.0747, from the flight path while minimising the power draw of the motor, yielding a final energy consumption of 11.588 kJ. Optimisation of the controller design parameters included mass and dynamic friction robustness studies' and a throttle saturation study. Alongside the implementation of multiple PID Tuning approaches such as Genetic algorithm and Ziegler-Nichols Rule.

Contents

List of Figures	iii
List of Tables	iv
List of Symbols	v
1 Multidisciplinary Design Approach	1
1.1 Motor Selection	1
2 Structural Design	1
2.1 Problem Specification	1
2.2 Stage 1: Sizing Optimisation	2
2.3 Stage 2: Topology Optimisation	2
2.4 Stage 3: Heuristic Refinement	3
2.5 FEA Verification	3
2.6 Eiger Print Settings	3
3 Control Law Design	4
3.1 Stage 1: System Dynamic Model	4
3.1.1 Mass and Friction Models	4
3.1.2 Acceleration and Velocity boundary conditions	4
3.1.3 Thrust and Power Curves	4
3.1.4 Throttle Saturation	5
3.1.5 Physics Model Validation	5
3.1.6 Simulating LiDAR Readings	5
3.2 Stage 2: Controller Design and Tuning Methodology	5
3.2.1 Controller Selection Exploration	5
3.2.2 PID Tuning Methodologies	5
3.2.3 Filter Tuning	6
3.2.4 Robustness Study	6
3.3 Stage 3: Final Sample Mission Profiles	7
4 Final Cost	7
5 Conclusion	7
References	8
A Project Flowchart	9
B Stage 1: Sensitivity Study	10
C Stage 2: Topology Optimisation	13
D Eiger Print Settings	15
E Final FEA Results	16
F Free Body Diagrams	20
G Thrust and Power models	20
H Free-Fall Model	22

I Physics Model Simulink & Code	23
J Closed Loop Model	26
K PID Tuning Rule	27
L Genetic Algorithm PID Tuning Optimisation	29
M Multiple PID Setup and Optimised Values	31
N Heat Map Plots	32
O Mission Profiles	33

List of Figures

1	Design Timeline	1
2	Heuristic modifications on motor housing	3
3	Mass and Dynamic Friction Robustness Study	6
4	Final mission profiles for Single and Two PID controller Designs with added noise	7
5	EP2 Duocopter Project Flowchart	9
6	Fitted curve of power vs thrust	10
7	Initial beam model	11
8	Width modification	11
9	Taper angle modification	11
10	Thickness modification	11
11	Sensitivity Study	12
12	Minimising strain energy for VF = 0.38	13
13	Convergence of optimisation parameters	13
14	Performance index for varying VF	14
15	Cubic spline overlay of mesh body in Fusion 360	14
16	Final Eiger Left	15
17	Final Eiger Right	15
18	Stress response, $\sigma = 11.70$ MPa [ABAQUS]	16
19	Stress response, $\sigma = 12.419$ MPa [Fusion 360]	16
20	Deflection response, $\delta = 2.649$ mm [ABAQUS]	17
21	Deflection response, $\delta = 2.815$ mm [Fusion 360]	17
22	Buckling response, 1st mode, $P_{crit} = 34.68$ N [ABAQUS]	18
23	Buckling response, 1st mode, $P_{crit} = 33.15$ N [Fusion 360]	18
24	Rotated and centered image	20
25	Power and Thrust Curve Fitting LC3536-7T	21
26	Throttle Saturation Study	21
27	Free-Fall Simulation	22
28	Simulink Block Diagram of the Physics Model	23
29	Closed Loop Model with noise and signal selector	26
30	Multiple PID layout	31
31	RMSE Heat Map, ($K_D = 20$) and ($K_D = 25$)	32
32	RMSE Heat Map, ($K_D = 30$) and ($K_D = 35$)	32
33	Step Up Mission Profiles with added noise	33
34	Step Down Mission Profiles with added noise	34
35	Sine Mission Profiles with added noise	34
36	Climb Mission Profiles with added noise	34

List of Tables

1	Motor System Specifications, (including ESC and Propeller)	1
2	FEA Verification	3
3	Final Single PID Gains From Genetic Algorithm with defined bounds (lower, upper)	6
4	Thrust vs Power Curve Coefficients LC3536-7T	10
5	Mesh Sensitivity Study: Tip Deflection vs. Mesh Size	19
6	Thrust Curve Coefficients LC3536-7T	20
7	Power Curve Coefficients LC3536-7T	20
8	Final Two PID Gains From Genetic Algorithm	31
9	Signals Testing	33

List of Symbols

A	Accuracy
b	Width
C	Cost function
E	Young's Modulus
F_r	Frictional force
h	Height
I	Moment of inertia
K_d	Derivative gain
K_i	Integral gain
K_p	Proportional gain
L	Arm length
L_c	Length of cart
L_{cg}	Weight moment arm relative to the rails
L_t	Thrust moment arm relative to the rails
M	Mass
N_f	Normal reaction force
P	Power
P_{cr}	Critical Buckling load
$RMSE$	Root Mean Squared Error
S	Cost Scoring
S_T	Throttle setting
T	Thrust
u	Throttle command
VF	Volume Fraction
W	Energy
δ	Deflection
\ddot{h}	Acceleration
\dot{h}	Velocity
μ	Coefficient of friction
σ	Bending Stress
σ_{SF}	Bending Stress Safety Factor
τ	Shear Stress
θ	Tip deflection slope
C_{df}	Coulomb coefficient of dynamic friction

1 Multidisciplinary Design Approach

The goal of this project was to design, build and test the structure and controller of a 1 degree-of-freedom (1-DOF) Duocopter. Primary objectives were: minimising manufacturing cost, power consumption and RMS error from a flight plan. Equation 1 was used in both the structural and control law design process. The aim was to minimise this cost function with respect to energy consumed, controller accuracy and manufacturing cost. The link between structural and controller design were seen through the optimisation of key global parameters, such as mass, that affect both the cost to print and the open loop response of the system. Thus a multidisciplinary approach was applied to the project, aiming to optimise both structural and controller design in parallel as much as possible. Figure 1 and Figure 5 outlines the methodology followed.

$$C = f(Energy, Mass, Accuracy) = 0.3W + 0.3M + 0.4A \quad (1)$$

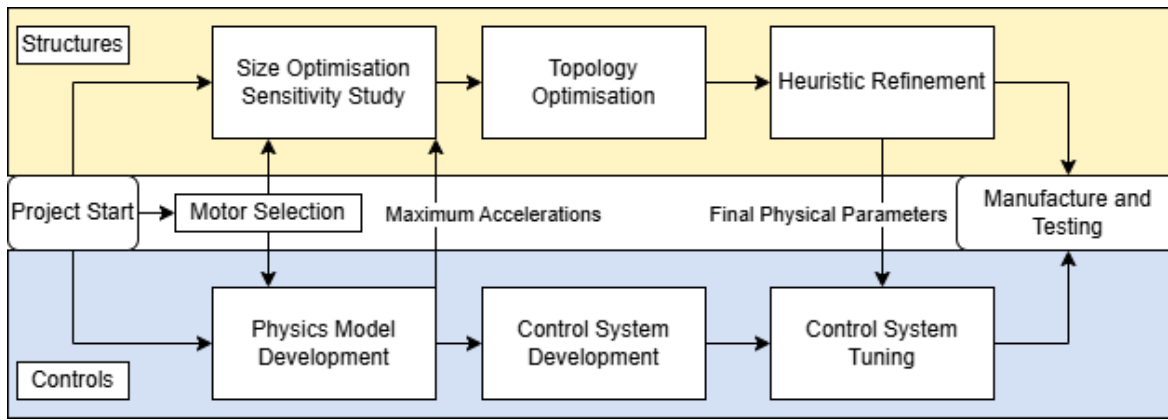


Figure 1: Design Timeline

1.1 Motor Selection

To select the optimal motor, both power and mass specific thrust were compared between the two models provided. Table 1 outlines these metrics alongside the total mass for each case including the motors, ESC and propellers. To minimise energy consumption, both power and mass specific thrust should be maximised. From this requirement the LC3536-7T was selected since it outperforms in both of these performance metrics.

Table 1: Motor System Specifications, (including ESC and Propeller)

Motor System	Power specific Thrust [m ⁻¹ s]	Mass specific Thrust [ms ⁻²]	Total Mass [g]
LC2835-4T	0.03427	61.947	124
LC3536-7T	0.03580	77.443	164

2 Structural Design

2.1 Problem Specification

The goal of the structural design was to design the cheapest arms possible while maintaining δ_{max} of less than 3.18 mm (accounting for safety factor and cost function weighting) and a minimum stress safety factor of 1.5 as is typical for aerospace structural applications [1]. In order to achieve this, the problem was simplified by modelling the arm as a solid, isotropic beam, fixed at the bottom where it is mounted to the carriage and pinned at the top to join with the second arm. A dovetail joint, with an angle of 15 degrees, was chosen for its high strength application and ability to resist in plane bending moments [2]. An initial width, thickness and taper angle of 50 mm, 10 mm and 0° respectively was chosen. The motor housing was placed on the centre line of the block to avoid effects of eccentric loading, modelled as a square with the specified mounting holes. The full setup can be seen in Figure 7.

2.2 Stage 1: Sizing Optimisation

Initial optimisation consisted of four parameter sweeps to identify the optimal width, taper angle and thickness of a simplified beam. Fusion 360 was used to conduct static load analysis to find the effect of these parameters on the key performance metrics: mass, deflection and safety factor. The load case was modelled as a concentrated force of 12.68 N applied at the centre of the motor housing. As the SIMP topology optimisation algorithm in Abaqus allows for a single objective function only (in this case to minimise compliance, subject to a VF constraint), if performed on an unoptimised geometry, it often suggests unfeasible geometries hence sizing optimisation was conducted first. To quantify the results, a scoring function was derived in terms of mass, tip deflection and stress SF. Structural mass was found to be directly proportional to the print time and global cost. The effect of tip deflection was found from Mohr's theorem, relating the slope of the beam to the thrust output with Equation 2. Assuming deflection is proportional to the slope when small and by fitting the power output to the thrust, a quadratic relationship was obtained as seen in Figure 6. Therefore, tip deflection was given a weighting proportional to its square. The final scoring function was found as Equation 3.

$$\theta = \int_0^L \frac{-TL}{EI} dx = \frac{-TL^2}{EI}, \therefore \theta \propto -T \quad (2)$$

$$S = f(M, \delta, \sigma_{SF}) = \Delta\delta^2 + \Delta M + \Delta\sigma_{SF} \quad (3)$$

Increasing beam width decreased the maximum deflection. This is reflected in the cube power law for beam bending theory as seen in Equation 12. However, beyond a width of 80 mm, the safety factor decreased, indicating an optimal width between 50 - 70 mm as shown in Figure 8. Ultimately, 60 mm scored highest and was used in subsequent studies. Increasing taper angle (Figure 9) reduced mass and increased safety factor, following a linear relationship. A taper angle of 6° was found to be optimal. From the final parameter sweep, it was seen that decreasing beam thickness seen in Figure 10 resulted in lower mass while causing a higher δ . A thickness of 8 mm scored highest and was chosen for stage 2. Moreover, offsetting the motor mount by 10 mm lets the arm be printed on its side, reducing the volume of plastic used by 50%, according to the Eiger preview. However, this introduces eccentric loading, increasing the torsional force on the arms and reducing the buckling safety factor. This was considered an acceptable compromise since out of plane reinforcements can be added to combat these effects. Details on the sensitivity study and FEA results are shown in Figure 11 and Appendix D respectively.

2.3 Stage 2: Topology Optimisation

Following the sensitivity study, SIMP based topology optimisation was conducted in Abaqus to identify regions where material could be removed. The primary goal of this stage was to reduce mass whilst maintaining high stiffness. As such, the objective function was specified to minimise the strain energy (i.e compliance) with a constraint on the VF. This was varied from 0.2 - 0.4 in 4% increments to identify a design that represents an acceptable trade off between tip deflection, which reduces with reduced compliance, and mass, a function of VF. Preserve regions were constructed surrounding the boundary conditions (holes to mount to carriage and dovetail joint) as well as the motor housing to ensure secure fits across the arm.

Equation 1 was used to compute the score of each VF design to produce Figure 14, with a maximum of the curve found for VF = 0.38 converged Figure 13. This design was chosen for the final arm and its mesh body (seen in Figure 12) imported to Fusion 360 for re-creation. An inherent uncertainty in the re-creation of rough iso-surfaces is that STL mesh bodies do not retain faces that can be used as direct sketch planes, hence cubic spline interpolation was performed to approximate the shape while maintaining continuous curvature to avoid meshing and print errors.

2.4 Stage 3: Heuristic Refinement

The topology optimised arm underwent a buckling analysis and identified, through trial and error, that conic profiles connecting the motor hosing to the main arm profile could reinforce the arm laterally: leading to an increase in the buckling safety factor from 1.78 to 2.65. Figure 2 highlights the difference in pre and post webbing structures, with FEA results for this heuristic modification found in Appendix D. Though the final safety factors are higher than the 1.5 industry standard [1], they were deemed acceptable due to the assumption of isotropic material for simulations and 3D printing imperfections.

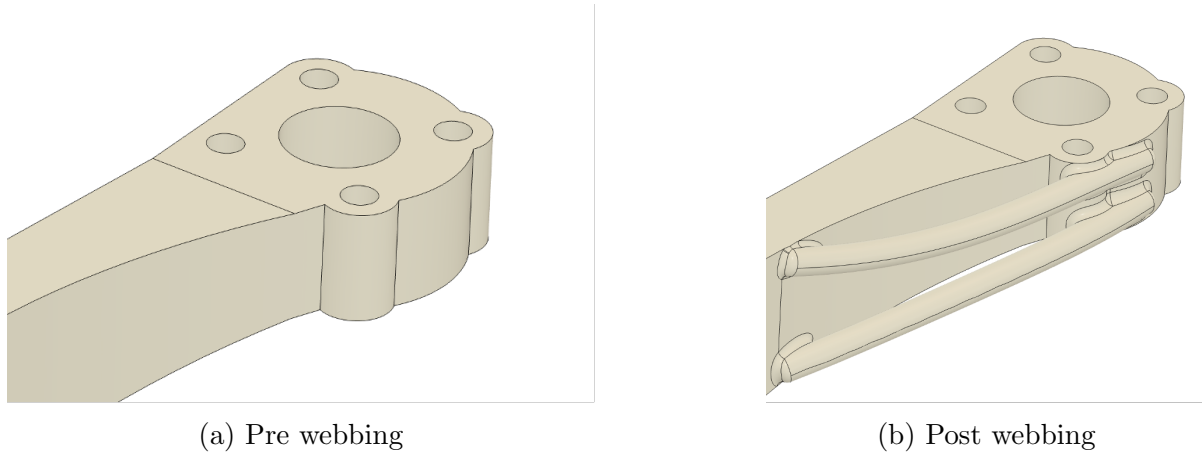


Figure 2: Heuristic modifications on motor housing

2.5 FEA Verification

FEA analysis was conducted on the final design in Fusion 360 and Abaqus to verify the stress and buckling safety factors alongside maximum tip deflection and torsional forces. Full stress and deflection heatmaps can be found in Appendix D. A concentrated force of 12.68 N was applied to the motor housing, tied with an kinematic coupling constraint from the centre of the 10 mm clearance hole to the four 3.2 mm mounting holes. Treating the motor as a rigid body, the thrust from the motor is distributed across these mounting holes into the frame, making this an appropriate model of the load case. Moreover, a torsional moment of 5.28 Nmm was applied to model the torque effect of the contra-rotating motors about the vertical Z axis. Table 2 displays key performance metrics and the relative error between the two software, with a low mean error relative to Abaqus of 5.64%, indicating confidence in the results obtained. A mesh independence study can be found in appendix Appendix D where a global mesh size 2 was used in both Abaqus and Fusion. It was found that mesh seeds below 1 were converged to within 3 decimal places, thus it was used as a reference for other seeds. From this, a mesh seed of 2.4 was used for further simulations as it has a relative percentage difference of less than 1%.

Table 2: FEA Verification

Software	σ_{SF}	Buckling SF	δ [mm]	Mean Percentage Error [%]
Fusion 360	4.10	2.61	2.82	5.64
Abaqus CAE (2024 edition)	4.35	2.74	2.65	N/A

2.6 Eiger Print Settings

With reference to Eiger's print settings guide [3], a gyroid pattern was chosen for it's ability to resist both shear and torsional loads, in addition to it's high resistance to out of plane forcings. An infill percentage of 40, 5 floor layers and 2 wall layers provided a suitable balance of print time vs strength with the wall thickness in particular of 0.8 mm being at least 20 % of the inner webbing thickness of the arm.

3 Control Law Design

3.1 Stage 1: System Dynamic Model

Considering the forces acting on the system results in Equation 4.

$$\ddot{h}M_{inertia}(h) = T(S_T) - F_r(T, \dot{h}, M_g(h)) - M_g(h)g \quad (4)$$

The inertial mass is the mass of the moving system while gravitational mass is the mass the duocopter has to lift, both are functions of height. The thrust is simply a function of the throttle setting and the friction being a function of thrust, mass and velocity. This was modelled in Simulink as shown in Figure 28.

3.1.1 Mass and Friction Models

The mass model consists of the gravitational and inertial masses stated previously. Fundamentally, they are a sum of the constant masses and the mass of the power and control cables, that hang from the bottom of the cart, which increases with height. This is illustrated in Equation 5.

$$M_g(h) = M_{constant} + M_{cables}(h) = M_{arms} + M_{motors} + M_{ESCs} + M_{cart} + M_{cables}(h) \quad (5)$$

As seen on the datasheet [4] for the rails, the mass of the assembled carriage is 0.4 kg. Thus, the inertial mass adds 0.8 kg to the gravitational mass as the main and counterweight carriage masses have to be considered. To model the mass of the cable with respect to height, both a catenary and a linear model was considered. To reduce processing time, the linear model shown in Equation 6 was applied, as coded in Listing 2. and a mass robustness study was conducted to ensure that the inaccuracies due to this model would not affect the accuracy.

$$M_{cables}(h) = \mu_{cables}(0.5h - 0.28) \quad (6)$$

The friction model is a piecewise function of velocity: at zero, a static friction of 130 g per carriage is used; otherwise, the Coulomb friction model: Equation 7 is used. C_{df} was set to 0.17, the given upper bound[5].

$$F_r = C_{df}N_f(T, M_g) \quad (7)$$

For Coulomb friction, the normal reaction force is a function of mass and thrust. It was defined by using distances shown in Figure 27 and moments to find the function shown in Equation 8 and coded in Listing 3.

$$N_f(T, M_g) = \frac{TL_t + M_ggL_{cg}}{L_c} \quad (8)$$

3.1.2 Acceleration and Velocity boundary conditions

When the duocopter is at the top of the rail, it is constrained and cannot accelerate or move upwards. This also applies at the bottom as the duocopter cannot fall further down. This is represented by if statements in Listing 4 and Listing 5, setting impossible accelerations and velocities to 0 when at the top or the bottom. The height is defined at zero when the cart is at rest on the bottom of the track and can reach a maximum height of 144 cm [5].

3.1.3 Thrust and Power Curves

The Thrust and Power provided by one motor was approximated by a 6th-order polynomial fit of the given data [5]. Where S_T is the percentage throttle command, T is the thrust of one motor in newtons and P is the power of one motor in watts. With $R^2 = 0.9982$ and $R^2 = 0.9969$ respectively, the polynomial fits represent an accurate model of the data. The Max Power was used to define the $W_{max} = 29.200$ kJ as a normalisation factor for the Cost function Energy. This was coded in MATLAB as shown in Listing 1.

$$T = (aS_T^6 + bS_T^5 + cS_T^4 + dS_T^3 + eS_T^2 + fS_T) \times 10^3 \quad (9)$$

$$P = (aS_T^6 + bS_T^5 + cS_T^4 + dS_T^3 + eS_T^2 + fS_T) \times 10^4 \quad (10)$$

3.1.4 Throttle Saturation

The upper limit was set to $S_T = 90\%$, this was chosen by inspecting the thrust curves, which topped out at approximately 90% throttle. Additionally a sensitivity study was conducted to find the ideal saturation point and how it correlated with RMSE and Energy Consumption, the findings showed that the RMSE was minimised at a saturation point of $S_T = 90\%$ Figure 26. A saturation block was used to limit excess power consumption which would have little effect on the max thrust of the motors, as seen in Figure 29.

3.1.5 Physics Model Validation

To validate the accuracy of the dynamic models, a free-fall experiment was conducted with the empty test rig. The cart took an average of 1.12 s to free-fall from 1.44 m to 0 m. Simulation using the physical model in Simulink indicated 1.0 s required with $C_{df} = 0.17$ [5]. The discrepancy between the results indicated an error in either the physics model or the experiment, requiring a friction robustness study.

3.1.6 Simulating LiDAR Readings

White noise following a Gaussian distribution ($\mu = 0, \sigma^2 = 10$), with a gain of 0.0005 [6] was added onto the signal during testing to simulate the experimental noise from LiDAR sensors. This allows the determination of the filter coefficient during tuning. A sample time of 0.05 s was used to emulate the setup of the testing rig to ensure similarity. This is displayed as the "Generate noise" subsystem of Figure 29.

3.2 Stage 2: Controller Design and Tuning Methodology

3.2.1 Controller Selection Exploration

To control a 1-DOF duocopter using only thrust, the choice of controller plays vital role in achieving robustness and good performance. Both Model Predictive Control (MPC) and Linear-Quadratic Regulator (LQR) have superior performance: faster execution time [7] and higher resistance to noise [8] in many scenarios [9] due to MPC's ability to incorporate future predictions [10] and LQR being robustly stable for the small modelling errors [11]. However both present challenges when applied to small scale, low-complexity systems.

3.2.2 PID Tuning Methodologies

Many methods were used to tune the controller using the sample mission [5] to allow comparison. The first being the Ziegler-Nichols PID tuning rule (Z-N) [12]. It requires a step input to a desired height (using 1 m to evaluate overshoot without hitting the boundaries); increasing the value of K_p until the output of the closed loop response has stable oscillations, while keeping K_i and $K_d = 0$ [13]. Z-N works well when the system is linear and monotonic [12]. Due to the non-linearity of the system, a sole- K_p controller could not produce the required consistent stable oscillations, causing Z-N to fail.

The second approach implemented was a Genetic Algorithm (GA). It optimises the PID and the derivative filter coefficient with the objective function as the RMSE. GAs offer a robust, population-based search for tuning PID controllers by encoding gains (K_p, K_i, K_d, N) as chromosomes, within defined bounds. Each candidate's fitness combines tracking accuracy, quantified by RMSE and energy, weighted to balance responsiveness and efficiency. Through selection, crossover, and mutation: successive generations evolve toward lower costs while preserving elite solutions. This method draws on Holland's GA principles [14] and PID tuning theory [15, 16], yielding automated, multi-objective optimization without requiring model linearity or gradient information. Its flexibility allows for use with multiple controller designs, such as Cascade and Adaptive PID models. The final results are summarised in Table 8.

Table 3: Final Single PID Gains From Genetic Algorithm with defined bounds (lower, upper)

$K_P(50, 300)$	$K_I(10, 150)$	$K_D(0, 100)$	$N(1, 20)$	RMSE	Energy [J]
112.95	33.89	28.54	14.77	0.0717	11588

Studies were conducted into using two PID controllers for different error thresholds ($u_{error} < 0.1$). The system was optimised for 8 parameters. The performance for the sample mission showed: $RMSE_{TwoPID} = 0.0602$ and, $Energy_{TwoPID} = 11359$ J. The Multi-PID setup had lower RMSE and Energy consumption than the single PID setup, performing better on sharp ascents and descents. However, the relative simplicity and speed of tuning the single PID setup, despite marginally higher Energy and RMSE scores, led us to use it for controller testing. The Multi PID characteristics are included in Appendix M.

Approach three was to do a grid search as shown in Listing 6 and heuristically refine the search region by plotting a heatmap over multiple iterations; Aiming to find a range of gains that minimise RMSE values. This was used to verify the results from other tuning methods. The data gathered confirmed the neighbourhood of PID values was similar to that of the GA Tuning. Results displayed in Appendix N.

3.2.3 Filter Tuning

The built-in derivative filter N was used to reduce the effects of noise and was optimised using a GA, yielding a value of 14.77. First-Order low-pass filters were considered in the design but they produced large time-delay effects that need to be countered by a delay block, risking the possibility of a negative response time.

3.2.4 Robustness Study

Studies were done to confirm controller stability if key physical parameters varied. $M_{constant}$ and C_{df} were varied by $\pm 20\%$ of the estimated values. There were minimal changes in the RMSE and Energy of the response signals due to variations in either coefficient, showing that the controller remained stable for most values within an appropriate variation of the physical parameters. The stability of the responses also shows the advantages of the simple PID controller, with its simplicity and robustness.

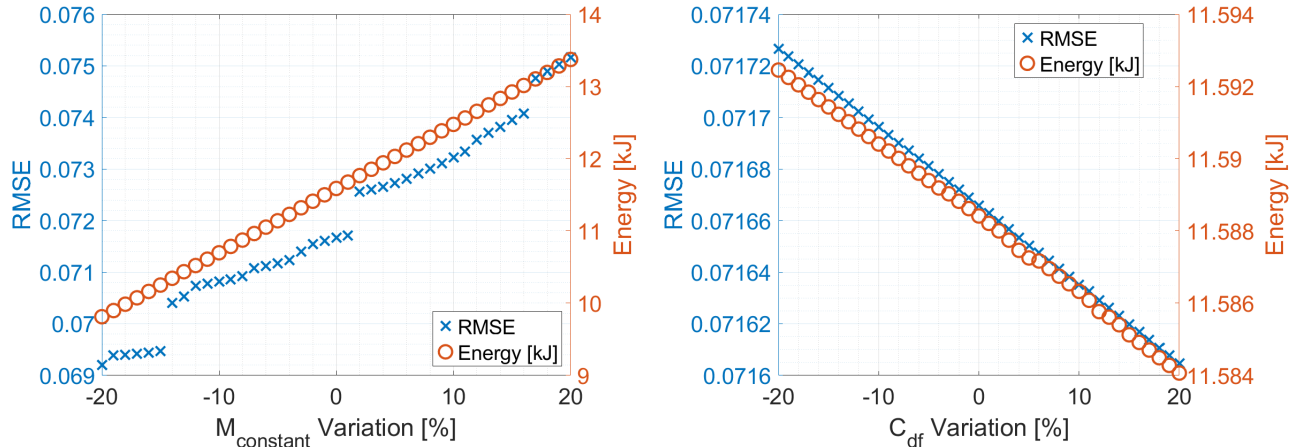
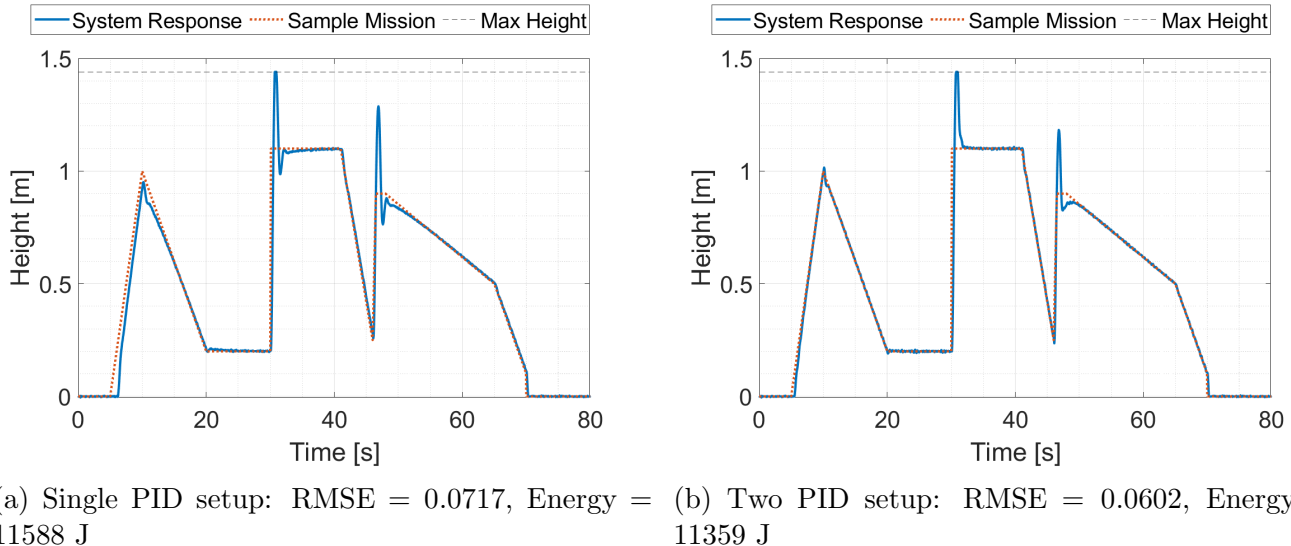
(a) Mass Variation Study $M_{constant} = 0.528$ kg (b) Dynamic Friction Coefficient Study $C_{df} = 0.17$

Figure 3: Mass and Dynamic Friction Robustness Study

3.3 Stage 3: Final Sample Mission Profiles

Final performance was evaluated using the sample mission [5] with performance metrics displayed below. A range of additional signals, such as sinusoidal and step inputs, were tested for both PID setups in Appendix O. High overshoots can be seen; this can be explained by a quasi-steady assumption applied to the thrust model as the motor control input and the thrust will not be instantaneous and depends on the state of the duocopter.



(a) Single PID setup: RMSE = 0.0717, Energy = 11588 J (b) Two PID setup: RMSE = 0.0602, Energy = 11359 J

Figure 4: Final mission profiles for Single and Two PID controller Designs with added noise

4 Final Cost

Following from the cost function Equation 1, energy and mass were normalised by $W_{max} = 29,200 \text{ kJ}$, derived from the maximum power consumption of one motor, and $M_{min} = 0.045 \text{ kg}$, obtained from iteration 17 of the sizing optimisation table Figure 11. The final normalised cost is displayed in Equation 11

$$C_{predicted} = 0.3 \times \frac{11.588kJ}{2 \times 29.200kJ} + 0.3 \times \frac{0.050kg}{0.045kg} + 0.4 \times 0.0717 = \mathbf{0.4215} \quad (11)$$

5 Conclusion

The design of the arm was split into three stages of development, beginning with a heuristic parameter sweep of key geometric variables including the width, taper angle and thickness, followed by topology optimisation to identify redundant volume and final manual refinements to improve torsion and buckling performance. Performance indices and cost functions were used throughout to identify favourable designs measured against mass, safety factors and deflection. At each stage it was identified that the optimal solution was achieved not through design optimisation algorithms or heuristic modifications alone, but through the interplay of both working in parallel to create a better design than each method could achieve in isolation.

The design of the controller also used a combination of algorithmic and heuristic methods to tune the final PID gains. Initially, equations of motion for the system were derived, serving as the base for a SIMULINK model, which was validated with free-fall tests. Multiple controller designs and PID Tuning methodologies were explored, optimising for the lowest RMSE = 0.0717 and energy = 11.588 kJ, alongside the time efficiency of the tuning method. The relative simplicity and ease of tuning offered by a simple PID controller made it the best candidate for the duocopter controller, alongside a genetic algorithm tuning method to tune the controller gains. Robustness studies showed small variations from the ideal case. Testing with different signals indicated good performance in different flight plans. This indicates a robust and reliable controller.

References

- [1] Burr JBCAH. Mechanical Analysis and Design by Burr and Cheatham. 2nd ed. USA: Prentice Hall; 1995.
- [2] Company TTTM. 9 Types of Wood Joints – The Best Methods for Joining Wood; 2025. Available from: <https://www.tomaco.co.uk/9-types-of-wood-joints-the-best-methods-for-joining-wood/#:~:text=The%20best%20ways%20to%20join%20wood%20include%20techniques%20such%20as, and%20disadvantages%20in%20woodworking%20projects>.
- [3] Markforged. 3D Printing Settings Impacting Part Strength; 2025. Available from: <https://markforged.com/resources/learn/design-for-additive-manufacturing-plastics-composites/understanding-3d-printing-strength/3d-printing-settings-impacting-part-strength>.
- [4] Igus. DryLin® W - Harnessed DryLin® Systems;.
- [5] Quino G, Armanini S. Engineering Practice 2 – DBT Exercise; 2025.
- [6] Armanini S, Quino G, of Aeronautics D, London IC. sampleH.mat; 2025.
- [7] Benotsmane R, Kovács G. Optimization of Energy Consumption of Industrial Robots Using Classical PID and MPC Controllers. Energies. 2023 /1;16(8):3499. Available from: <https://www.mdpi.com/1996-1073/16/8/3499>.
- [8] Sharma R, Pfeiffer CF. Comparison of control strategies for a 2 DOF helicopter. 271-279. 2017. Available from: <https://openarchive.usn.no/usn-xmlui/handle/11250/2466980>.
- [9] Mosaad MI. Direct power control of SRG-based WECSs using optimised fractional-order PI controller. IET Electric Power Applications. 2020;14(3):409-17. Available from: <https://doi.org/10.1049/iet-epa.2019.0194>.
- [10] Mathworks. What Is Model Predictive Control?;. Available from: <https://uk.mathworks.com/help/mpc/gs/what-is-mpc.html>.
- [11] He JB, Wang QG, Lee TH. PI/PID controller tuning via LQR approach. Chemical Engineering Science. 2000 -07-01;55(13):2429-39. Available from: <https://www.sciencedirect.com/science/article/pii/S0009250999005126>.
- [12] Laboratories M. Ziegler-Nichols Tuning Rules for PID. Available from: <https://www.mstarlabs.com/control/znrule.html#Ref2>.
- [13] Ziegler JG, Nichols NB. Optimum Settings for Automatic Controllers. Journal of Dynamic Systems, Measurement, and Control. 1993 -06-01;115(2B):220-2. Available from: <https://doi.org/10.1115/1.2899060>.
- [14] Holland JH. Adaptation in natural and artificial systems : an introductory analysis with applications to biology, control, and artificial intelligence. 1st ed. Cambridge, Mass: MIT Press; 1992. Includes bibliographical references (pages 203]-205) and index.; ID: alma999936650001591.
- [15] Åström KJ HT. PID Controllers: Theory, Design, and Tuning; 1994.
- [16] Goldberg DE. Genetic Algorithms in Search, Optimization and Mahcine Learning. 2nd ed.; 1989.

A Project Flowchart

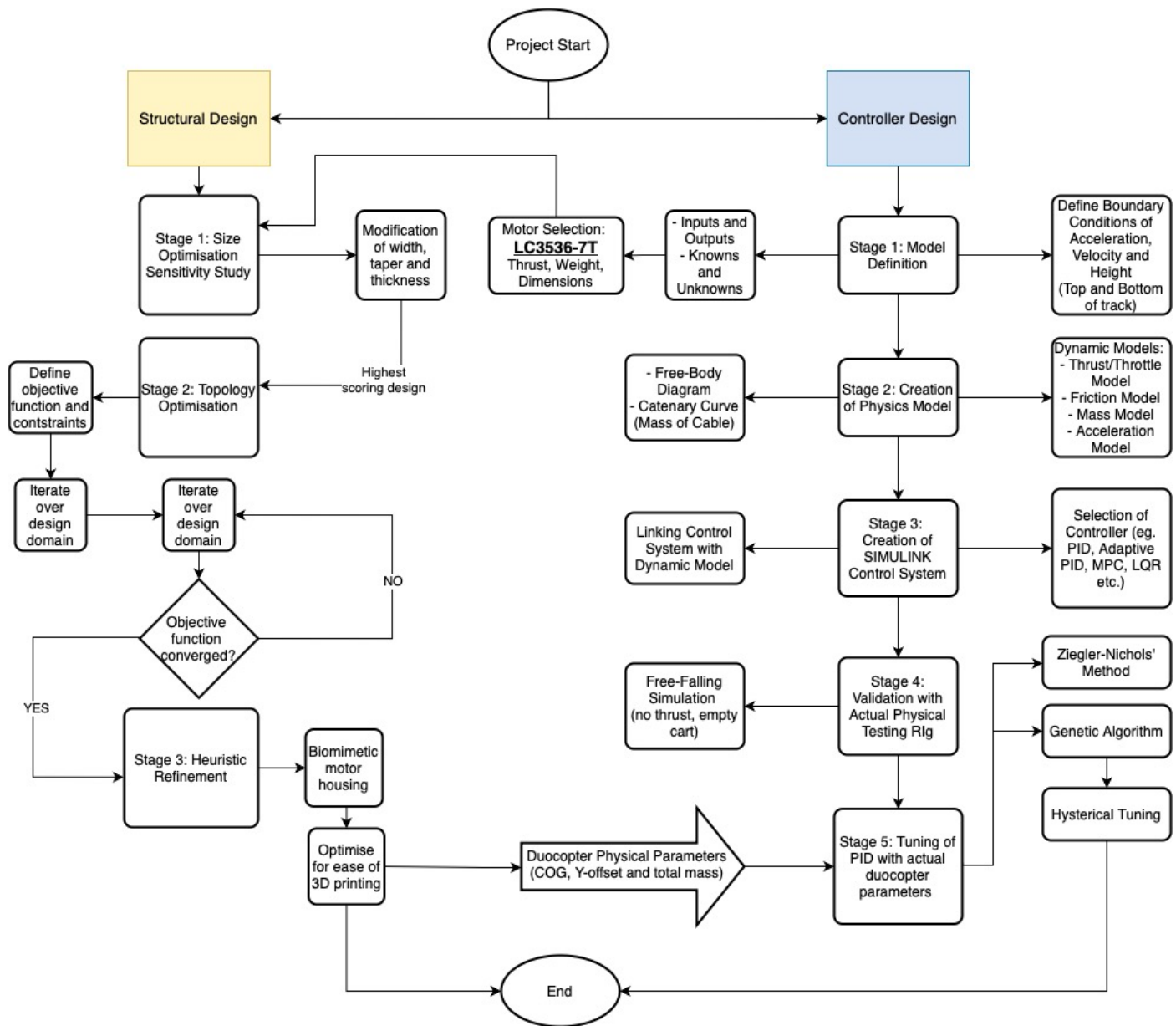


Figure 5: EP2 Duocopter Project Flowchart

B Stage 1: Sensitivity Study

$$P_{\text{cr}} = \frac{\pi^2 EI}{L^2} \quad (12)$$

$$I = \frac{bh^3}{12} \quad (13)$$

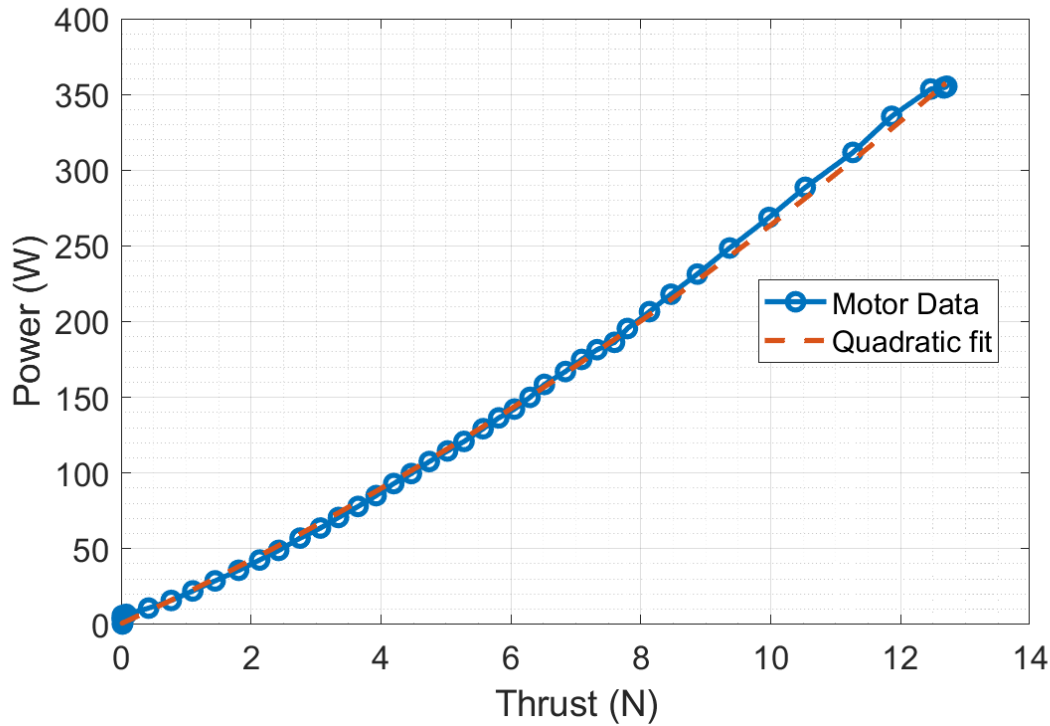


Figure 6: Fitted curve of power vs thrust

Table 4: Thrust vs Power Curve Coefficients LC3536-7T

$$P = aT^2 + bT + c \quad (14)$$

<i>a</i>	<i>b</i>	<i>c</i>	RMSE
0.666930	19.662402	0.444102	0.999526



Figure 7: Initial beam model



Figure 8: Width modification

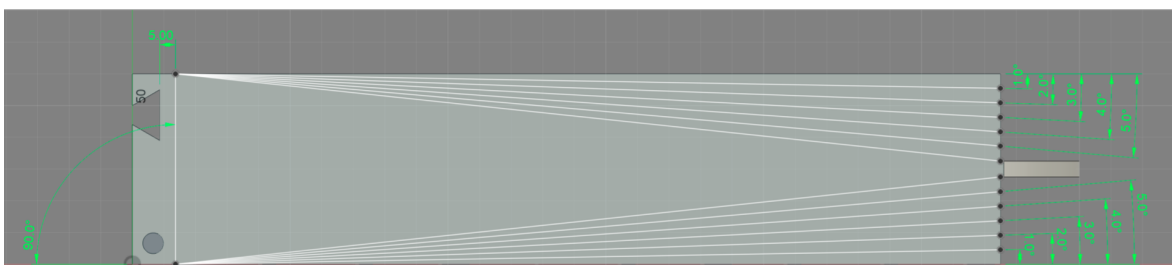


Figure 9: Taper angle modification

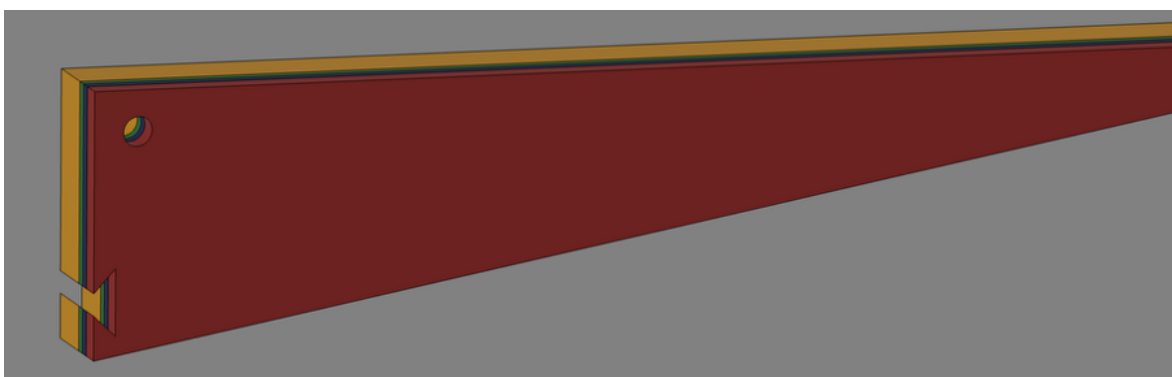


Figure 10: Thickness modification

	Width (mm)	Taper Angle (^o)	Thickness (mm)	Y-offset (mm)	Mass (g)	δ (mm)	σ_{SF}	Score	Observations	Modifier	(±)
	50	0	10	0	153.81	0.905	2.835	-4	As expected increasing the width of the beam decreases the maximum deflection, however surprisingly beyond a width of 80 mm the safety factor decreases, indicating an optimal width between 50 - 90mm. Ultimately 60mm chosen.	2	
	60	0	10	0	184.61	0.754	2.894	-0.8			
	70	0	10	0	215.41	0.678	2.877	-13.5			
	80	0	10	0	246.21	0.635	2.893	-42.29			1.5
	90	0	10	0	277.01	0.616	2.839	-96.1			1
12	60	1	10	0	171.258	0.79	2.836	7.7	Increasing the taper angle leads to a lower mass as expected, following a linear relationship. The max deflection increases as well however reinforcements can be used to reduce this for minimal mass regained. Safety factor for taper angle of 6 is highest.		
	60	2	10	0	157.898	0.826	2.836	13.8			
	60	3	10	0	144.521	0.879	2.844	2.1			
	60	4	10	0	131.12	0.965	2.835	-81.4			
	60	5	10	0	117.839	1.133	2.841	-18.8			
	60	6	10	0	104.118	1.825	2.899	-196.5			
	60	6	9	0	99.267	0.968	2.899	98.6			
	60	6	8	0	88.614	1.089	2.899	106.7			
	60	6	7	0	77.967	1.245	2.404	45.9			
	60	6	6	0	67.319	1.456	1.977	26.4			
B	60	6	5	0	56.561	1.734	1.711	24.6	Decreasing the beam thickness results in lower mass at the cost of max tip deflection, at a similar rate to when taper angle is modified. With consideration for out of plane buckling and durability, 8 mm is chosen for highest score and practicality for manufacturing.		
	60	6	4	0	45.914	2.164	1.484	-23			
	60	6	8	2	88.614	0.856	3	-4.7			
	60	6	8	4	88.614	0.895	3	-3.6			
	60	6	8	6	88.614	0.95	3	-2.1			
	60	6	8	8	88.614	0.993	3	-0.9			
	60	6	8	10	88.614	1.165	3	-14.3			
	60	6	8	12	88.614	1.428	3	-21.6			

Figure 11: Sensitivity Study

C Stage 2: Topology Optimisation

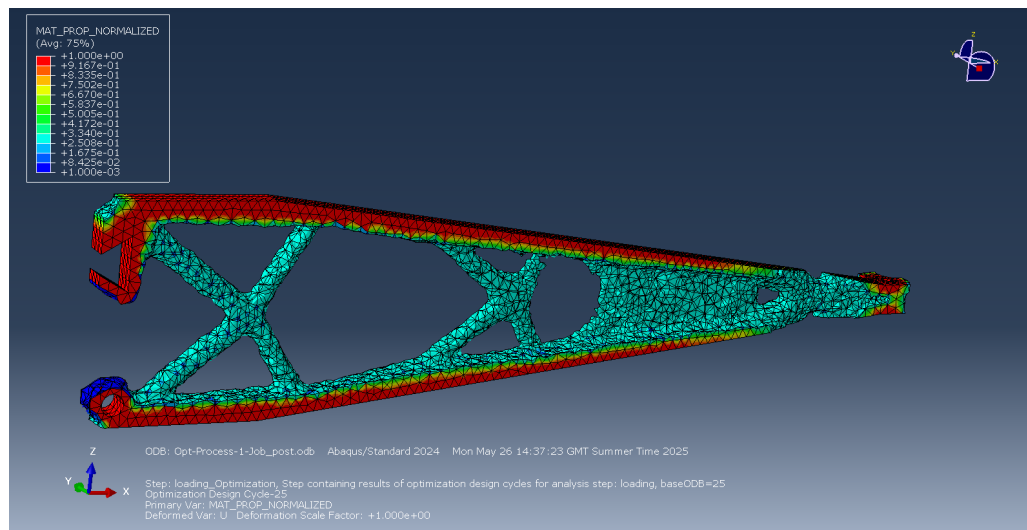


Figure 12: Minimising strain energy for VF = 0.38

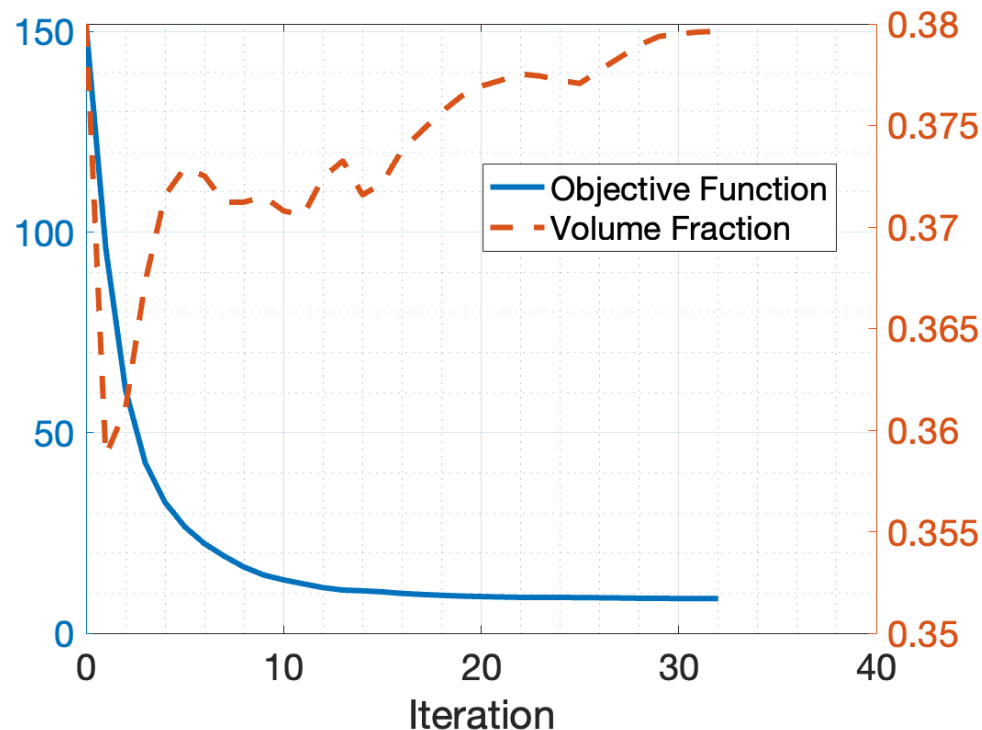


Figure 13: Convergence of optimisation parameters

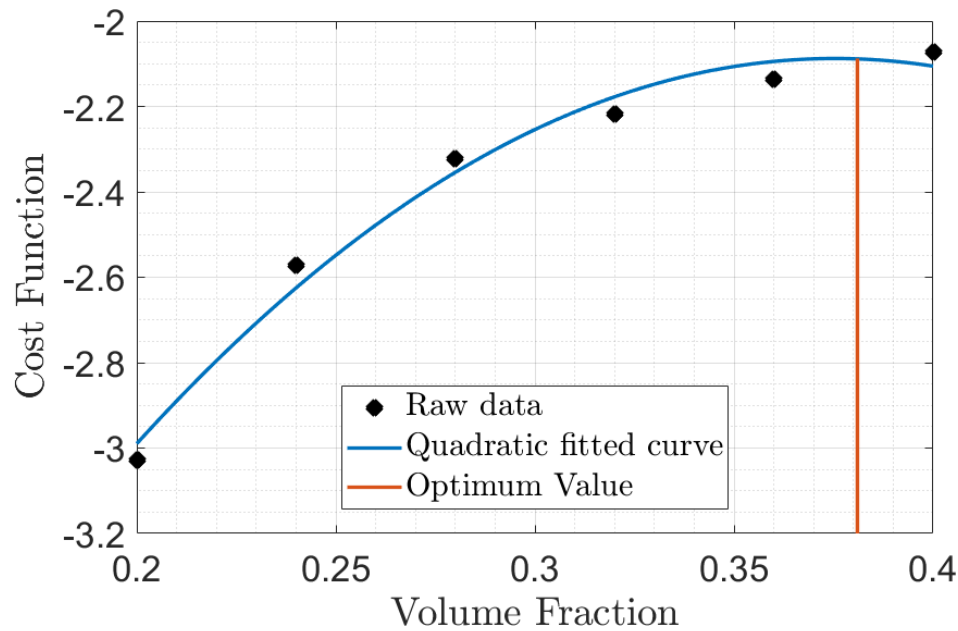


Figure 14: Performance index for varying VF

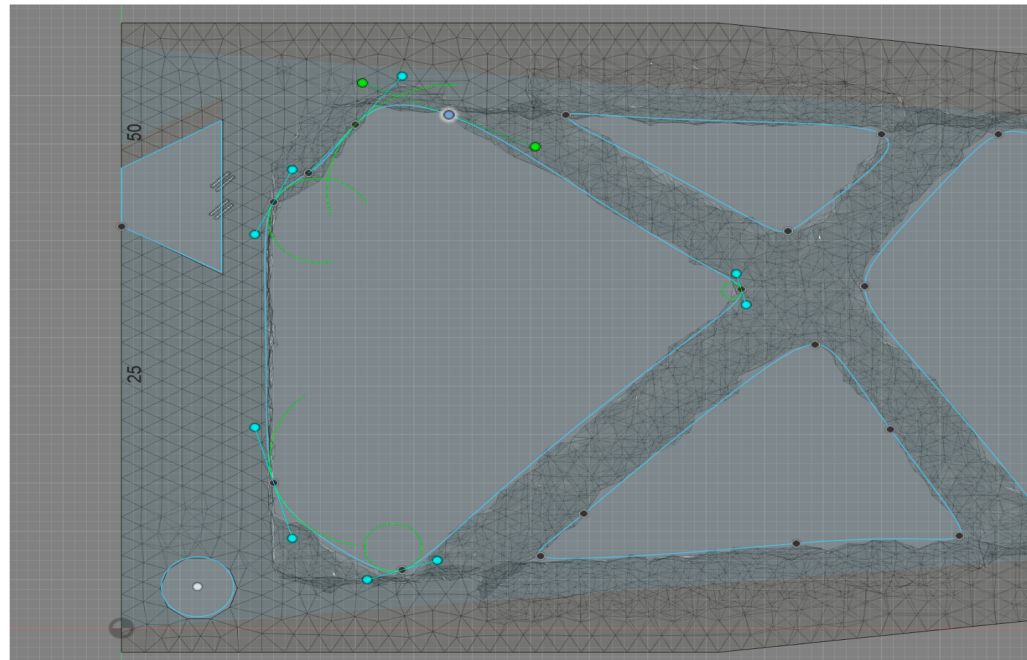


Figure 15: Cubic spline overlay of mesh body in Fusion 360

D Eiger Print Settings

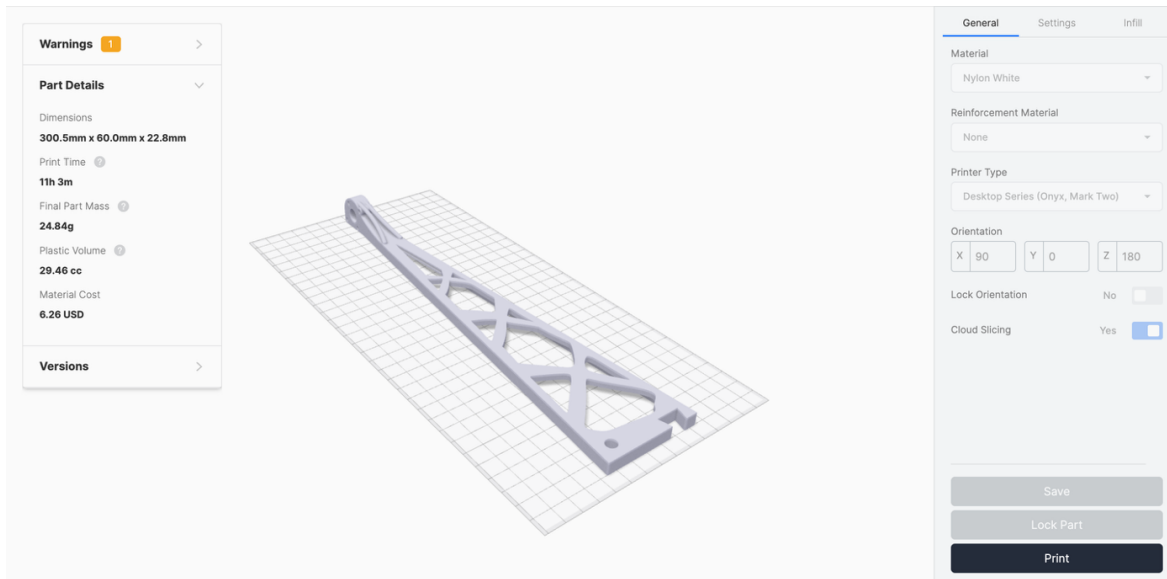


Figure 16: Final Eiger Left

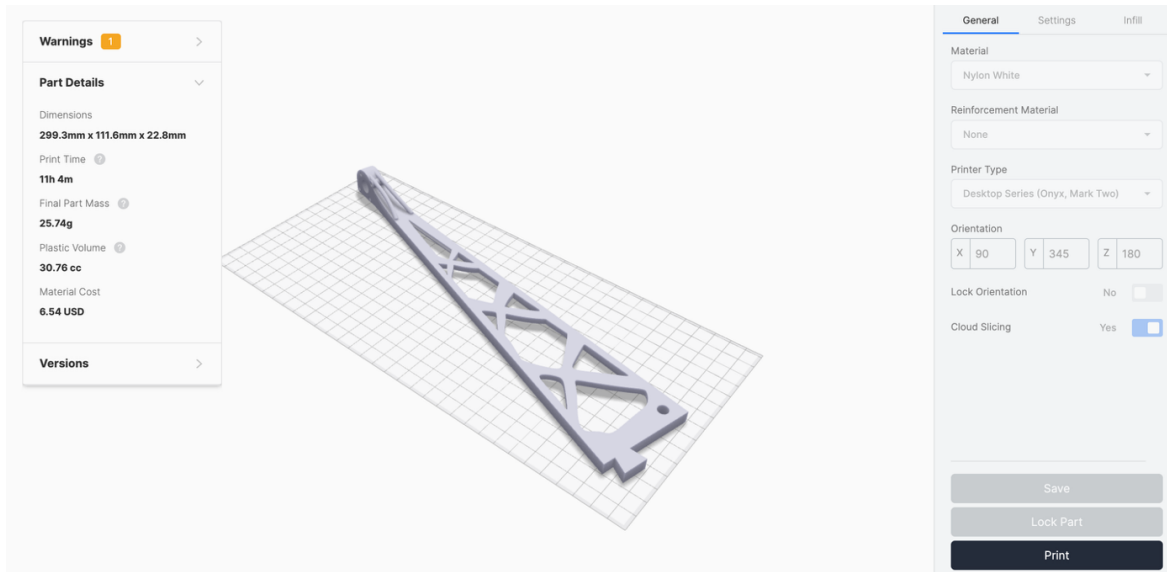


Figure 17: Final Eiger Right

E Final FEA Results

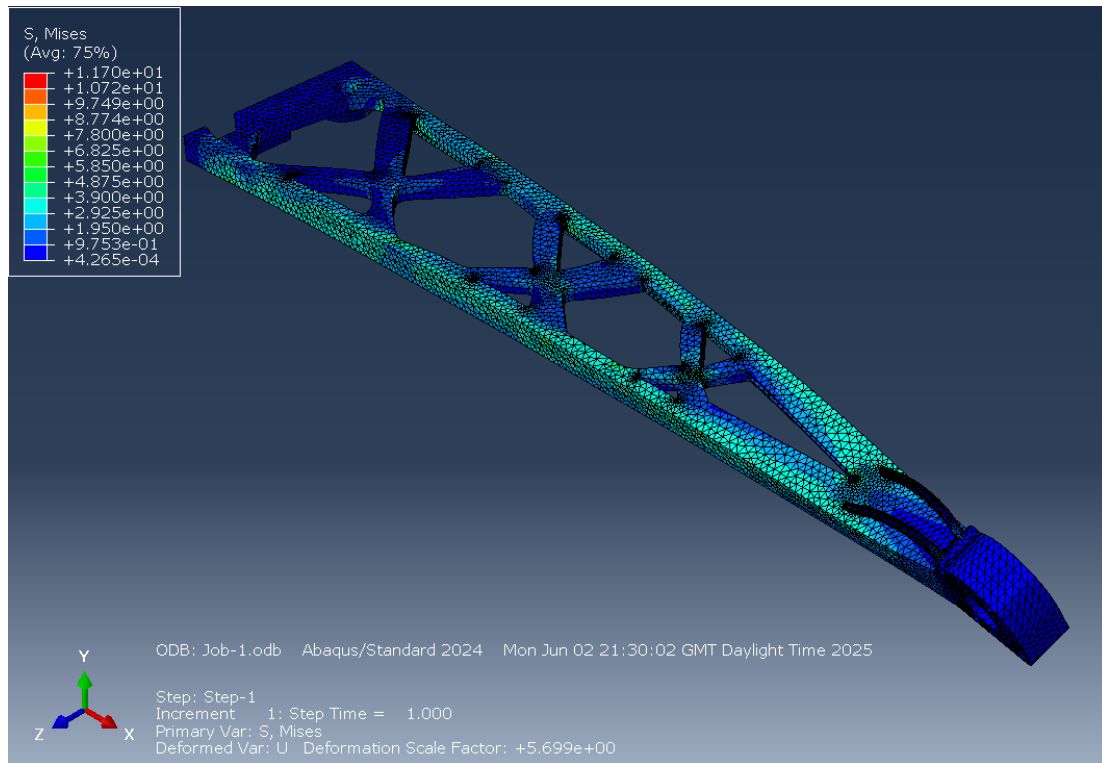


Figure 18: Stress response, $\sigma = 11.70$ MPa [ABAQUS]

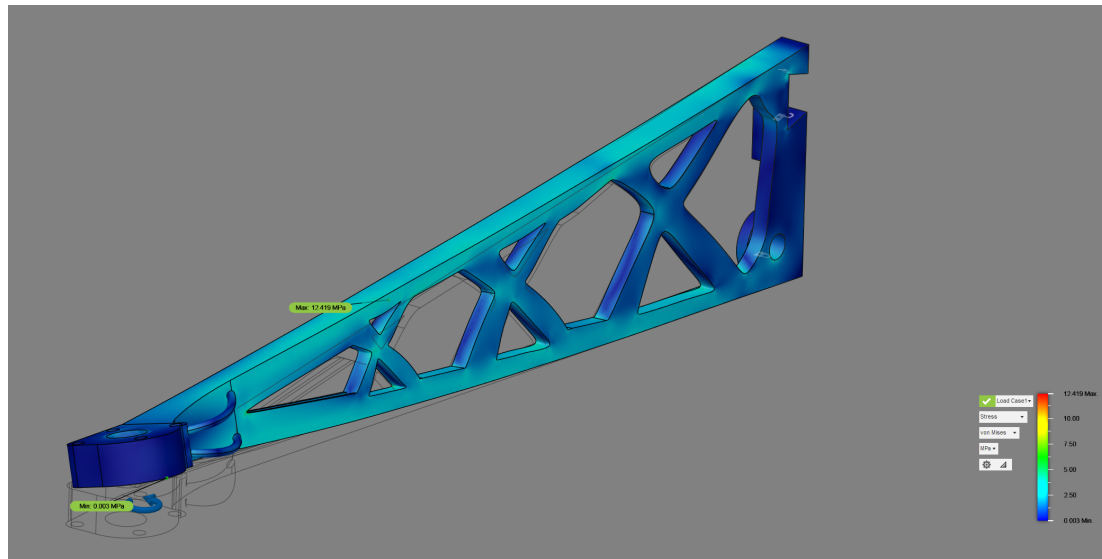


Figure 19: Stress response, $\sigma = 12.419$ MPa [Fusion 360]

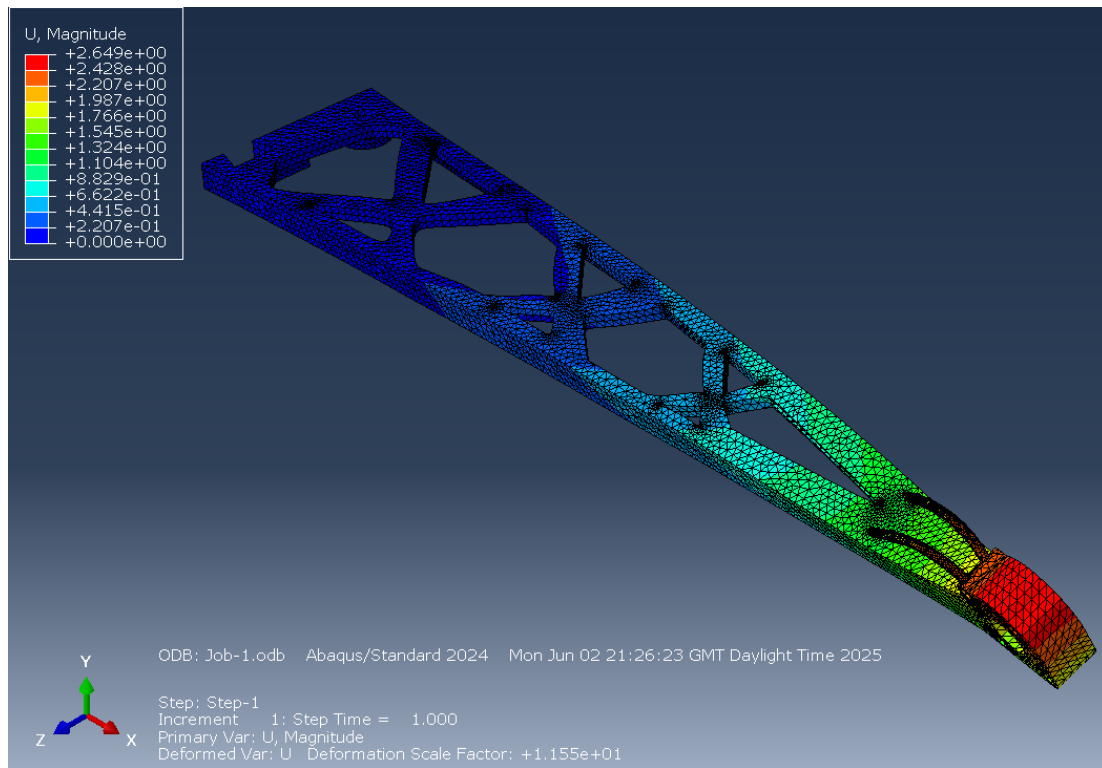


Figure 20: Deflection response, $\delta = 2.649$ mm [ABAQUS]

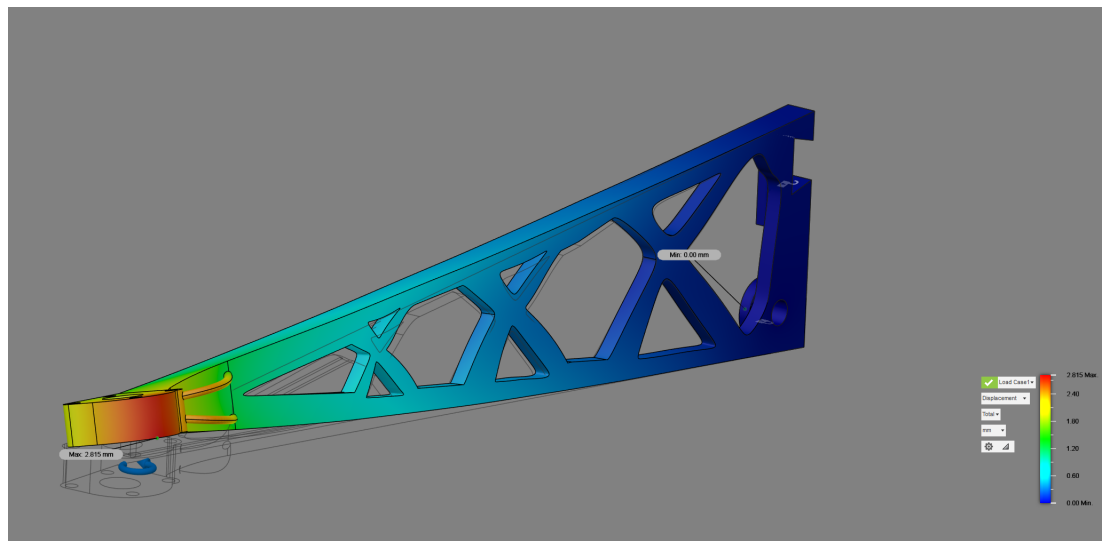


Figure 21: Deflection response, $\delta = 2.815$ mm [Fusion 360]

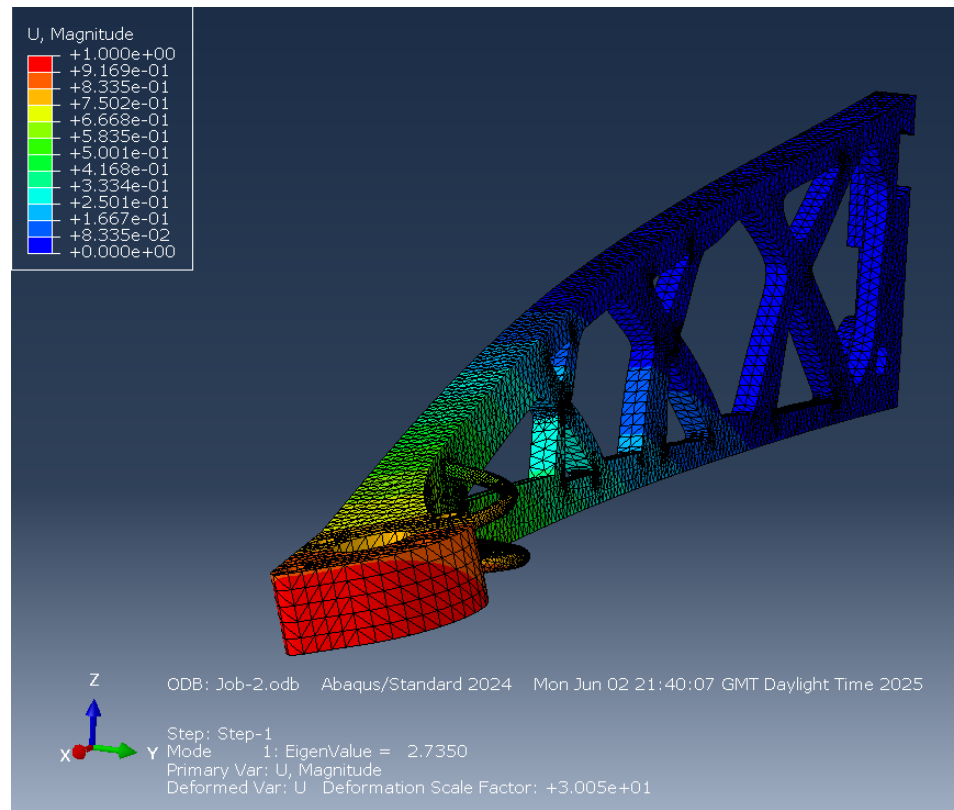


Figure 22: Buckling response, 1st mode, $P_{crit} = 34.68$ N [ABAQUS]

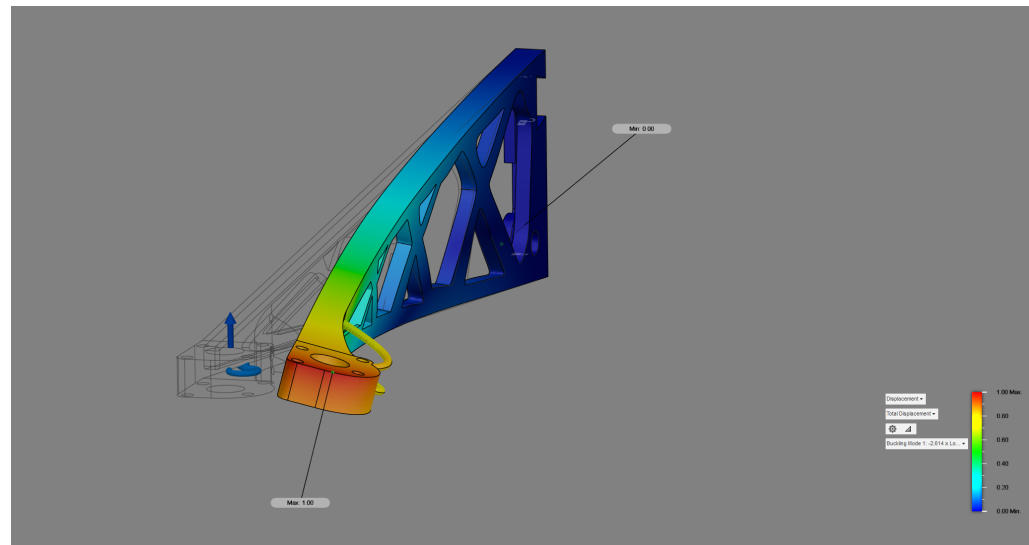


Figure 23: Buckling response, 1st mode, $P_{crit} = 33.15$ N [Fusion 360]

Table 5: Mesh Sensitivity Study: Tip Deflection vs. Mesh Size

Software	Mesh Size [mm]	δ [mm]	% Difference From Machine Epsilon
Fusion 360	3	2.800	1.16
	2.5	2.806	0.953
	2.4	2.807	0.918
	2.0	2.815	0.635
	1.0	2.833	0
Abaqus CAE (2024)	3.0	3.015	1.24
	2.5	3.086	1.08
	2.4	3.060	0.229
	2.0	3.051	0.0655
	1.0	3.053	0

F Free Body Diagrams

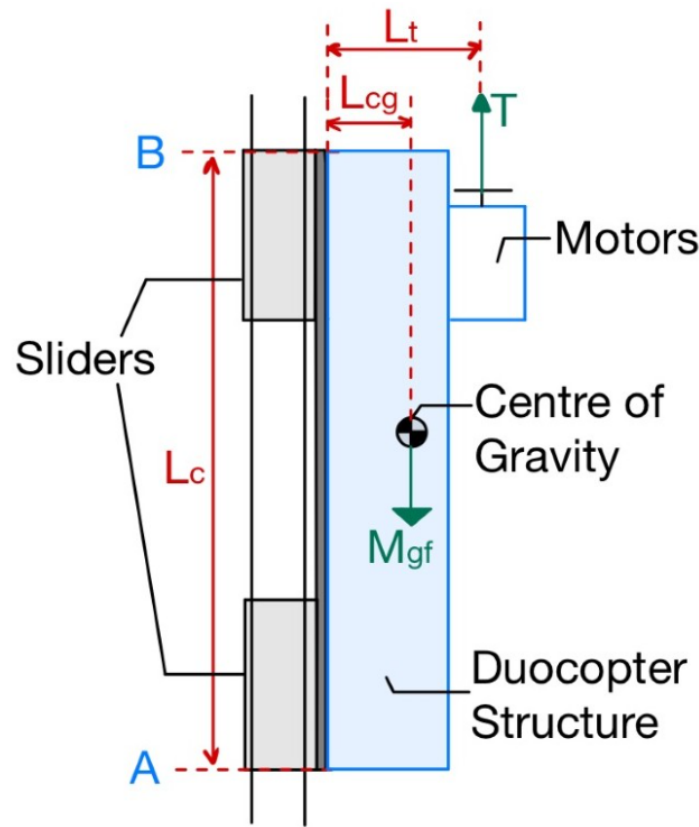


Figure 24: Rotated and centered image

G Thrust and Power models

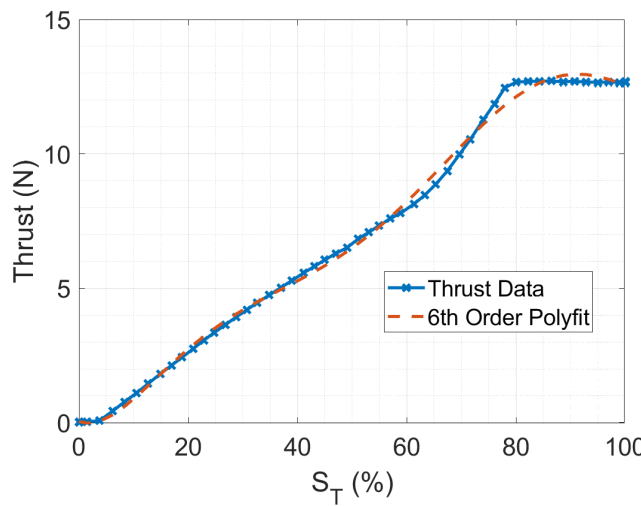
The Motor of choice was the LC3536-7T Motor with a mass of 114g.

Table 6: Thrust Curve Coefficients LC3536-7T

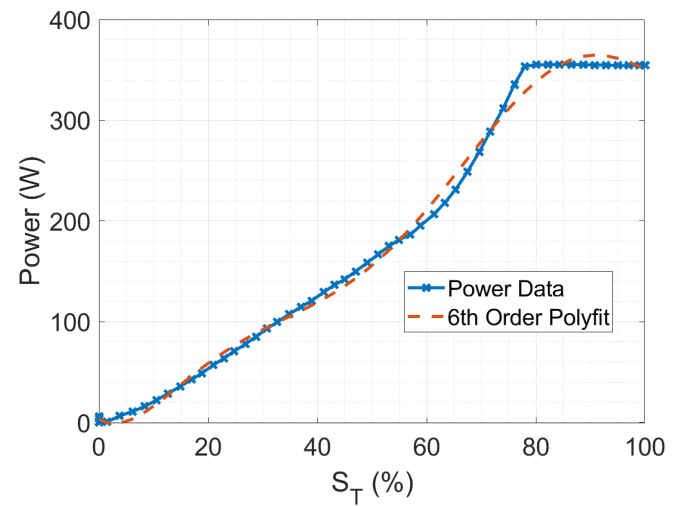
a	b	c	d	e	f	$RMSE$
0.451880	-1.486027	1.797219	-0.984319	0.241341	-0.007580	0.9982

Table 7: Power Curve Coefficients LC3536-7T

a	b	c	d	e	f	$RMSE$
1.401054	-4.543527	5.384918	-2.871959	0.697343	-0.033090	0.9969



(a) Thrust Curve LC3536-7T



(b) Power Curve LC3536-7T

Figure 25: Power and Thrust Curve Fitting LC3536-7T

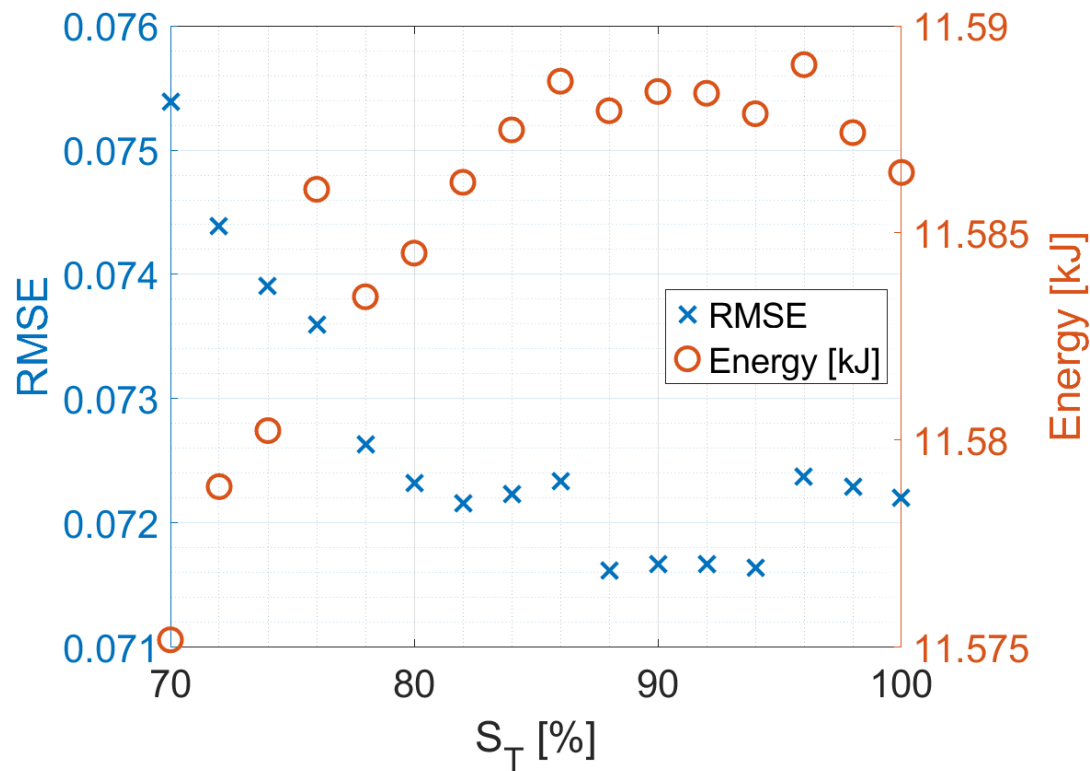


Figure 26: Throttle Saturation Study

H Free-Fall Model

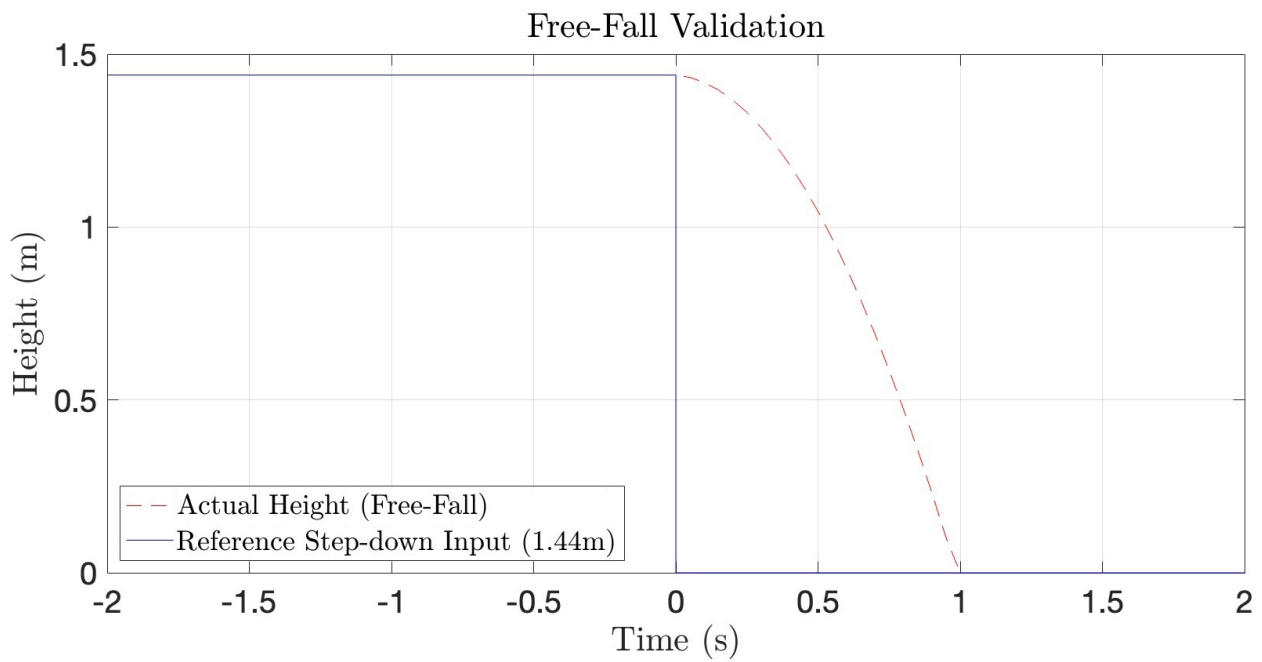


Figure 27: Free-Fall Simulation

I Physics Model Simulink & Code

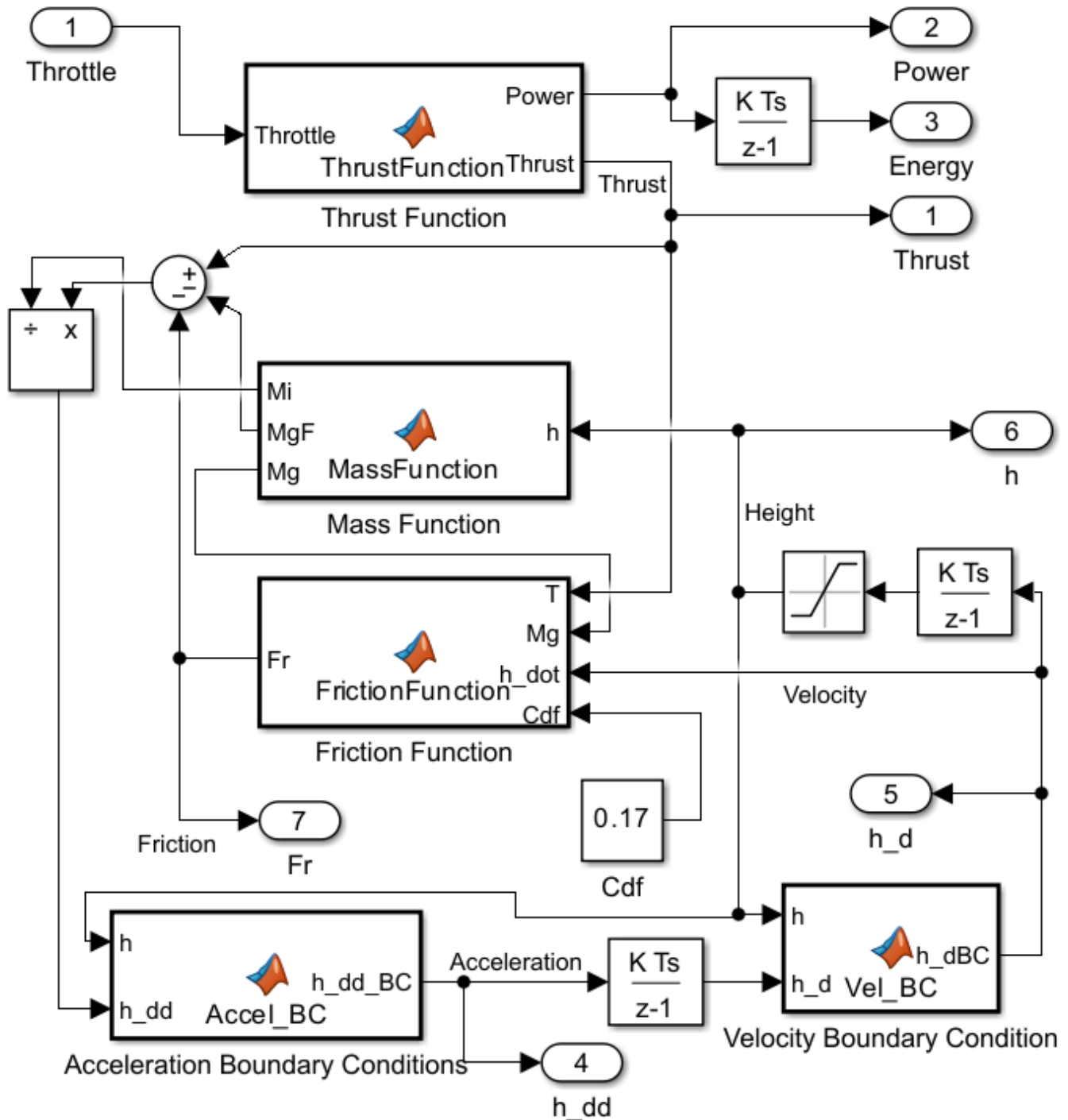


Figure 28: Simulink Block Diagram of the Physics Model

```

1 function [Thrust, Power ]= ThrustFunction(Throttle)
2
3 S_t = Throttle/100;
4
5 %Throttle to Thrust
6
7 % Polyfit 6th Order
8
9 a = 0.451880436962741;
10 b = -1.486027191210204;
11 c = 1.797219095509746;
12 d = -0.984318732289241;
13 e = 0.241341383767270;
14 f = -0.007579836329288;
15
16 Thrust = (2 * 1e+3) * (a*S_t^6 + b*S_t^5 + c*S_t^4 + d*S_t^3 + e*S_t^2 + f*S_t);
17
18
19 % Polyfit 6th Order
20
21 a = 1.401054302991919;
22 b = -4.543527223865324;
23 c = 5.384918481145972;
24 d = -2.871958912880594;
25 e = 0.697342980048495;
26 f = -0.033090224044331;
27
28 Power = (2 * 1e+4) * (a*S_t^6 + b*S_t^5 + c*S_t^4 + d*S_t^3 + e*S_t^2 + f*S_t);

```

Listing 1: Thrust and Power Function Code

```

1 function [Mi, MgF, Mg] = MassFunction(h)
2
3 %Given Masses in Kg
4 Mm = 0.328; %Motor Mass
5 Ma = 0.05; %Arm Mass
6 Mk = 0.15; %Cart Mass
7
8 M_constant = Mk + Mm + Ma;
9
10 Mc = 2*(0.095*h + 0.0532); %mass of cable is function of height
11
12 Mg = M_constant + Mc; %gravitational load
13 Mi = Mg + 0.8; % gravitational + carriage + counterweight
14
15 MgF = Mg * 9.81;

```

Listing 2: Mass Function MATLAB Code

```

1 function [FrStatic, Fr, N] = FrictionFunction(T, Mg, h_dot, Cdf)
2
3 l_t = 0.01; %Thrust Moment Arm
4 l_cg = 0.013922; %Centre of Gravity Moment Arm
5 l_c = 0.2104; %Length of carriage Moment Arm
6
7 FrStatic = 2 * 0.13 * 9.81;
8
9 N = abs((T * l_t - Mg * 9.81 * l_cg) / l_c); %Normal reaction force
10 % l_c * N = (T * l_t - Mg * 9.81 * l_cg) is moment equilibrium
11
12 if abs(h_dot) <= 0.2 %smallest measurable velocity is approx 0.2 m/s
13     Fr = FrStatic; %static friction
14 else
15     Fr = sign(h_dot) * Cdf * N; %dynamic friction
16     % note as friction is subtracted outside this block,
17     % it has to be calculated to be in the same direction of the velocity
18 end

```

Listing 3: Friction Function MATLAB Code

```

1 function h_dd_BC = Accel_BC(h, h_dd)
2 % Acceleration must be 0 at the top and bottom
3 if (h <= 0 && h_dd < 0) || (h >= 1.44 && h_dd > 0)
4     h_dd_BC = 0;
5 else
6     h_dd_BC = h_dd;
7 end

```

Listing 4: Acceleration Boundary Cases MATLAB Code

```

1 function h_dBC = Vel_BC(h, h_d)
2
3 if (h==0 && h_d < 0) || (h==1.44 && h_d > 0)
4     h_dBC = 0;
5 else
6     h_dBC = h_d;
7 end

```

Listing 5: Velocity Boundary Cases MATLAB Code

J Closed Loop Model

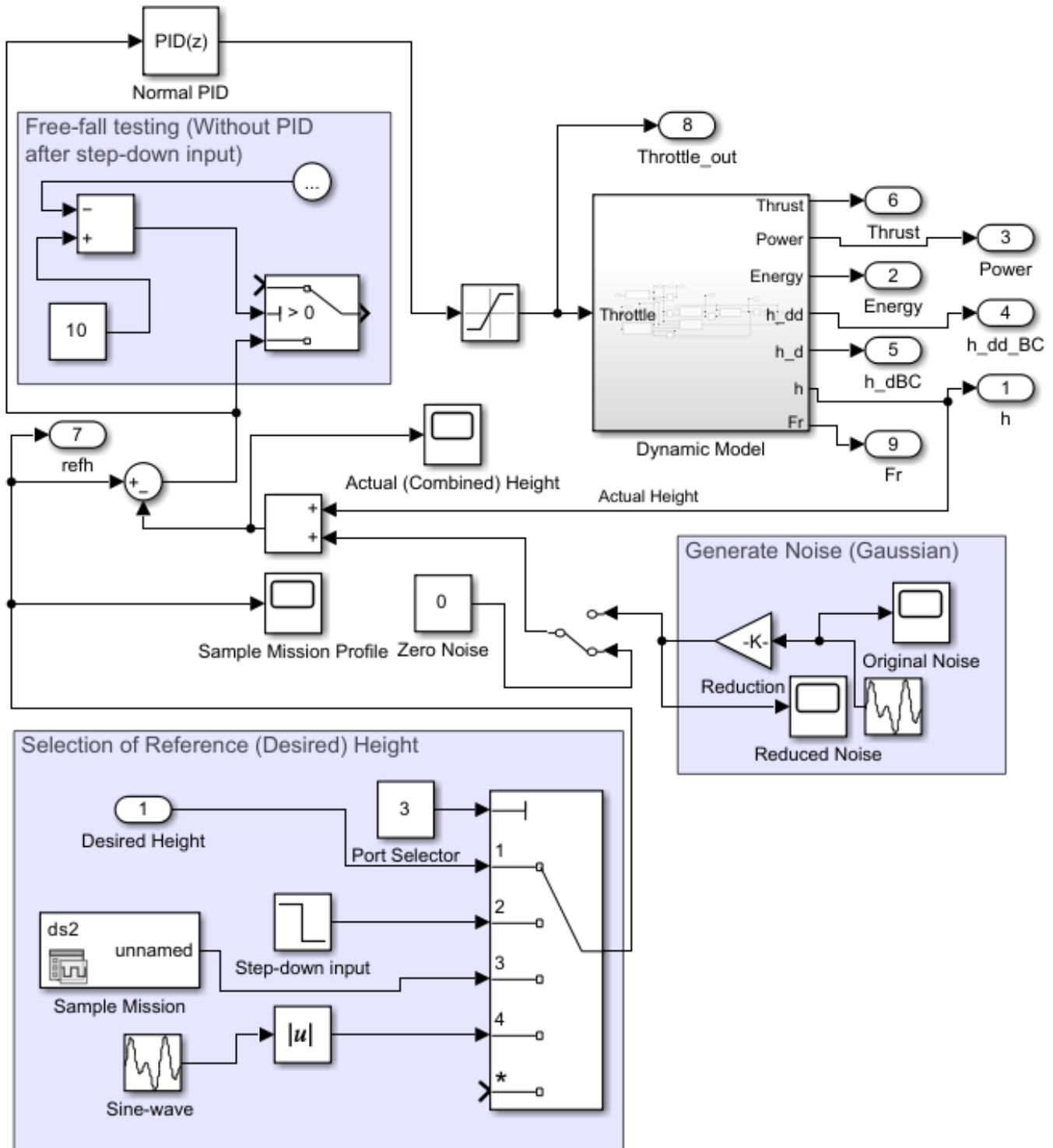


Figure 29: Closed Loop Model with noise and signal selector

K PID Tuning Rule

```

1 % initial set up
2 clear
3 clc
4 load ds2.mat % Sample Mission
5
6 model = "PID_Model_26May2025.slx";
7
8 open_system(model);
9
10 nP = 12; % number of Kp gridpoints to check
11 Kpl = linspace(195,201,nP); % Range of Kp values to search
12
13 nI = 10; % number of Ki gridpoints to check
14 Kil = linspace(18,23,nI); % Range of Ki values to search
15
16 nD = 5; % number of Kd gridpoints to check
17 Kdl = linspace(8,22,nD); % Range of Kd values to search
18
19
20 for p = 1:length(Kpl)
21     Kp = Kpl(p);
22
23     for i = 1:length(Kil)
24         Ki = Kil(i);
25
26         for d = 1:length(Kdl)
27             Kd = Kdl(d);
28
29             sm = sim(model, 'SimulationMode','normal','StopTime','80',...
30                     'SaveOutput','on','SaveTime','on');
31
32             RMSE(p,i,d) = sm.simout.Data(end);
33
34         end
35     end
36
37 % Manually save Kpl, Kil, Kdl and RMSE as a .mat file

```

Listing 6: Grid search MATLAB code

```

1 %initial set up
2 clc % clear command window
3 % do not clear workspace
4 % manually load Kpl, Kil, Kdl and RMSE arrays
5 % into workspace
6
7 % Select which Kdl slice
8 chosenslice = 4; % example: slice at Kdl(1)
9
10 % Extract 2D slice
11 Z_slice = squeeze(RMSE(:, :, chosenslice));
12
13 % Find minimum RMSE location
14 [min_val, min_idx] = min(Z_slice(:));
15 [row, col] = ind2sub(size(Z_slice), min_idx);
16 min_Kp = Kpl(row); % X axis (rows)
17 min_Ki = Kil(col); % Y axis (columns)
18
19 % Create meshgrid
20 [X, Y] = meshgrid(Kil, Kpl);
21
22 hold on;
23
24 % Plot heatmap
25 figure;
26 imagesc(Kpl, Kil, Z_slice);
27 set(gca, 'YDir', 'normal');
28
29 % Mark minimum point
30 plot(min_Kp, min_Ki, 'r*', 'MarkerSize', 10, 'LineWidth', 2);
31 text(min_Kp, min_Ki, sprintf(' Min: %.3f', min_val), 'Color', 'red', 'FontSize',
      , 10, 'FontWeight', 'bold');
32
33 % Labels and colorbar
34 colormap(parula);
35 colorbar;
36 xlabel('Ki');
37 ylabel('Kp');
38 title(['RMSE Heatmap at Kd = ', num2str(Kdl(chosenslice))]);
39
40 hold off;

```

Listing 7: Gridsearch Analysis MATLAB Code

L Genetic Algorithm PID Tuning Optimisation

```

1 %%%%%%%%%%%%%%%%%%%%%%%%%%%%%%%%%%%%%%
2 %% Author:   Himmat Kaul
3 %% CID:     02376386
4 %% Date:    28/05/2025
5 %%%%%%%%%%%%%%%%%%%%%%%%%%%%%%%%%%%%%%
6
7 % run_pid_ga.m
8 % Uses GA to optimize PID gains in Shank_PID_Model.slx
9
10 clear; clc; close all;
11
12 format long
13 s = settings;
14 s.matlab.fonts.editor.code.Name.TemporaryValue = 'Calibri';
15 set(groot,'defaultLineLineWidth',2) %sets graph line width as 2
16 set(groot,'defaultAxesFontSize',20) %sets graph axes font size as 18
17 set(groot,'defaultTextFontSize',20) %sets graph text font size as 18
18 set(groot,'defaultLineMarkerSize',8) %sets line marker size as 8
19 set(groot,'defaultAxesXGrid','on') %sets X axis grid on
20 set(groot,'defaultAxesYGrid','on') %sets Y axis grid on
21 set(groot,'DefaultAxesBox', 'on') %sets Axes boxes on
22
23 picturewidth = 20; % set this parameter and keep it forever
24 hw_ratio = 0.75; % feel free to play with this ratio
25
26 %% Genetic Algorithm Setup
27
28 % Define bounds for Kp, Ki, Kd N
29 lb = [0.1, 0.01, 0, 1]; % Lower bounds
30 ub = [300, 50, 30, 15]; % Upper bounds (tune as needed)
31
32 % 200 150 30 15
33
34 Cdf = 0.17;
35 M_test = 0.050;
36 mu_static = 0.26;
37
38 % Fitness function handle
39 fitnessFcn = @(x) pid_fitness(x);
40
41 % GA options
42 options = optimoptions('ga', ...
43     'Display', 'iter', ...
44     'PopulationSize', 30, ...
45     'MaxGenerations', 50, ...
46     'UseParallel', true, ...
47     'PlotFcn', {@gaplotbestf});
48
49 % Run GA
50 [x_opt, fval] = ga(fitnessFcn, 4, [], [], [], [], lb, ub, [], options);
51
52 fprintf('Optimized PID gains:\nKp = %.4f\nKi = %.4f\nKd = %.4f\nN = %.4f\n',
      x_opt);

```

```

53
54 % Save best gains
55 Kp = x_opt(1);
56 Ki = x_opt(2);
57 Kd = x_opt(3);
58 N = x_opt(4);
59
60 save('optimal_pid_gains.mat', 'Kp', 'Ki', 'Kd');
61
62 function cost = pid_fitness(x)
63     % Unpack PID values
64     Kp = x(1);
65     Ki = x(2);
66     Kd = x(3);
67     N = x(4);
68
69     % Assign to base workspace so Simulink can access
70     assignin('base', 'Kp', Kp);
71     assignin('base', 'Ki', Ki);
72     assignin('base', 'Kd', Kd);
73     assignin('base', 'N', N);
74
75 try
76     % Simulate the model
77     simOut = sim('Shank_PID_Model', ...
78                 'SimulationMode', 'normal', ...
79                 'StopTime', '80', ...
80                 'SaveOutput', 'on', ...
81                 'SaveTime', 'on');
82
83     % Extract output
84     y = simOut.get('y_out').signals.values;
85     t = simOut.get('y_out').time;
86
87     % Reference signal (assume step input to 1)
88     ref = ones(size(y));
89
90     % Compute error
91     e = ref - y;
92     Npts = length(e);
93     % Cost function: integral of squared error
94     cost = sum(e.^2)/Npts;
95
96 catch ME
97     % Print out what went wrong
98     fprintf('[!] Simulation failed: %s\n', ME.message);
99     cost = 1e6;
100
101 end
102 end

```

Listing 8: Genetic Algorithim PID Tuning Code

M Multiple PID Setup and Optimised Values

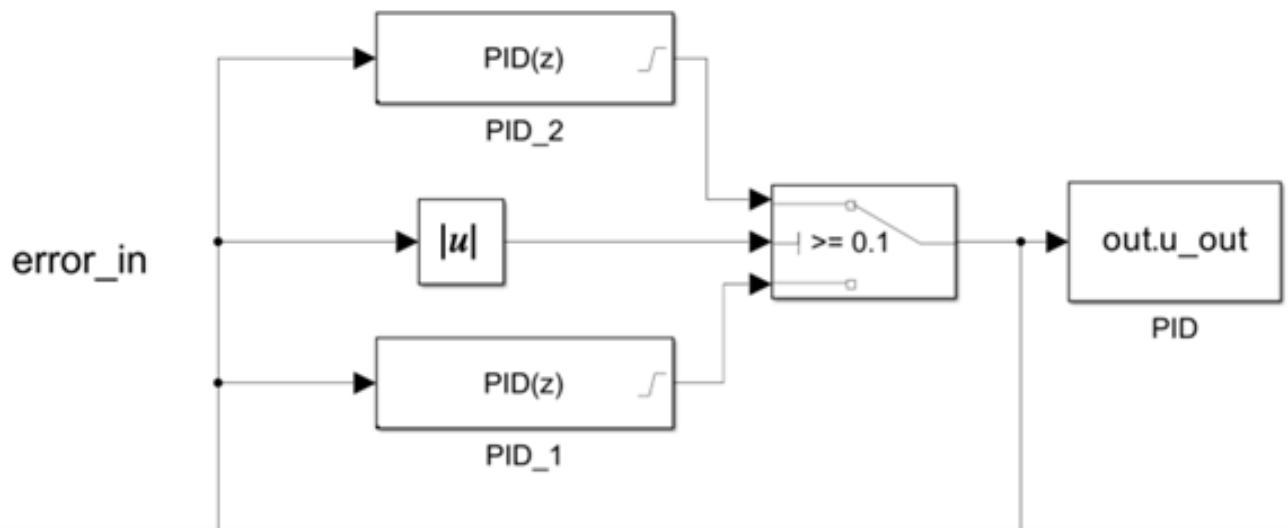
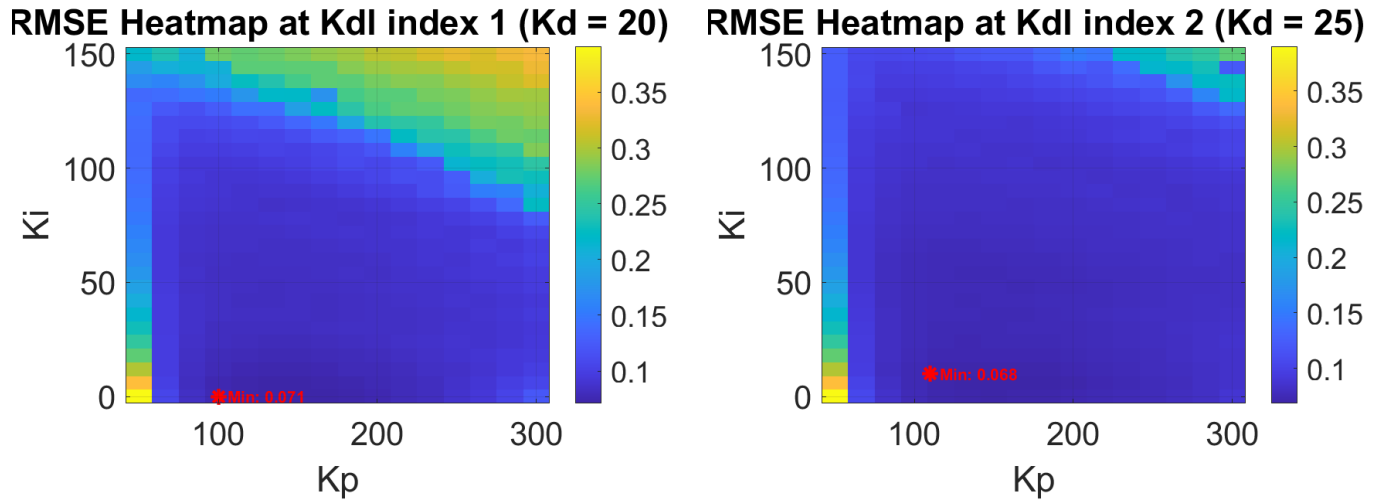


Figure 30: Multiple PID layout

Table 8: Final Two PID Gains From Genetic Algorithm

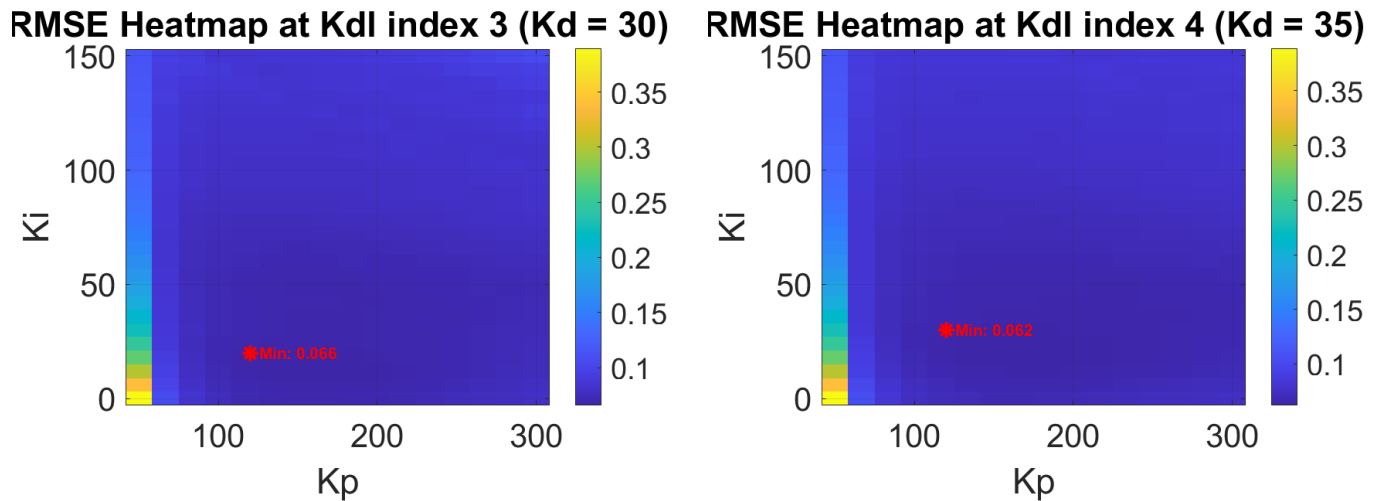
K_{P1}	K_{I1}	K_{D1}	N_1	K_{P2}	K_{I2}	K_{D2}	N_2	$RMSE$	$Energy$ [J]
(0.1,300)	(0.01,200)	(0,100)	(1,20)	(0.1,300)	(0.01,200)	(0,100)	(1,20)	-	-
226.75	199.89	51.32	16.60	241.64	137.70	70.28	19.51	0.0602	11359

N Heat Map Plots



(a) RMSE Heat Map at ($K_D = 20$), Minimum at ($K_P = 100, K_I = 0, RMSE = 0.071$) (b) RMSE Heat Map at ($K_D = 25$), Minimum at ($K_P = 110, K_I = 10, RMSE = 0.068$)

Figure 31: RMSE Heat Map, ($K_D = 20$) and ($K_D = 25$)



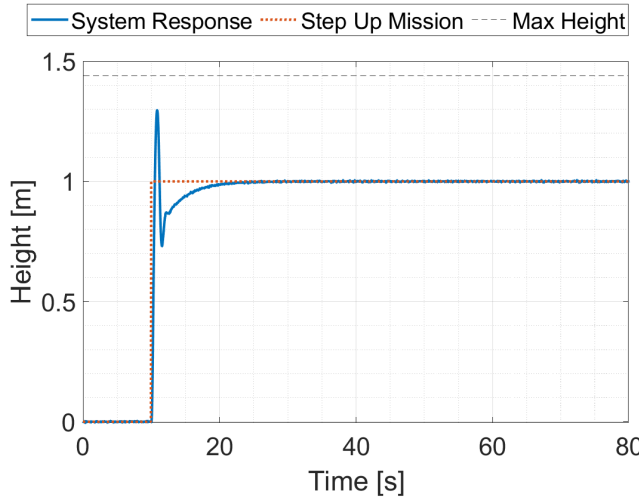
(a) RMSE Heat Map at ($K_D = 30$), Minimum at ($K_P = 120, K_I = 20, RMSE = 0.066$) (b) RMSE Heat Map at ($K_D = 35$), Minimum at ($K_P = 120, K_I = 30, RMSE = 0.062$)

Figure 32: RMSE Heat Map, ($K_D = 30$) and ($K_D = 35$)

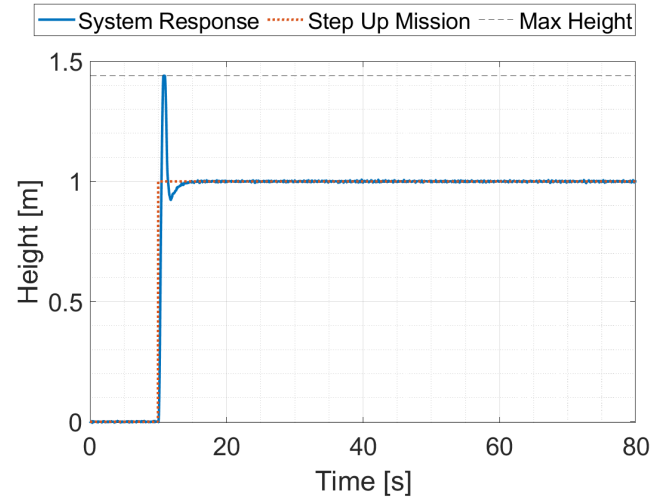
O Mission Profiles

Table 9: Signals Testing

	Single PID		Two PID	
Signal	RMSE	Energy [J]	RMSE	Energy [J]
Sample Mission	0.0717	11588	0.0602	11359
Step Up	0.0686	12104	0.0680	12141
Step Down	0.1422	3973	0.1794	14290
Sine Wave	0.0262	10363	0.0088	10731
Climb Mission	0.0486	10649	0.0362	10600

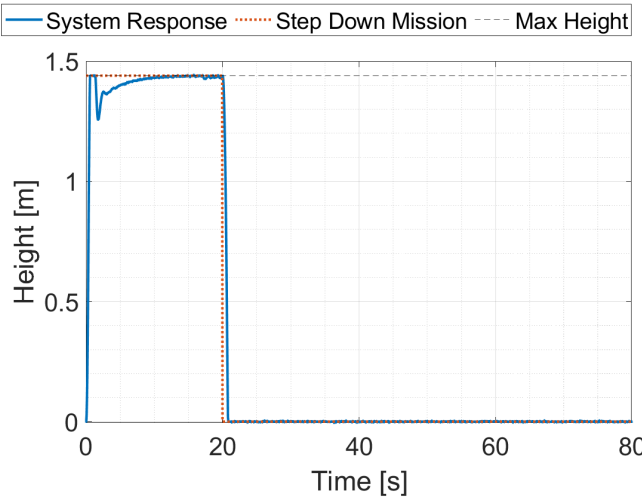


(a) Single PID Step Up

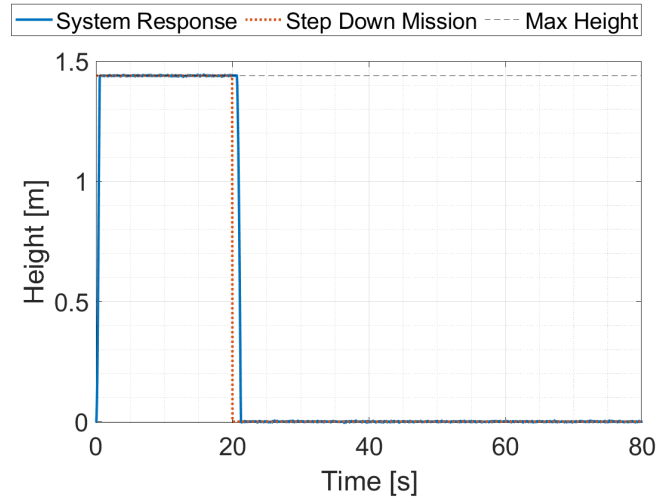


(b) Two PID Step Up

Figure 33: Step Up Mission Profiles with added noise

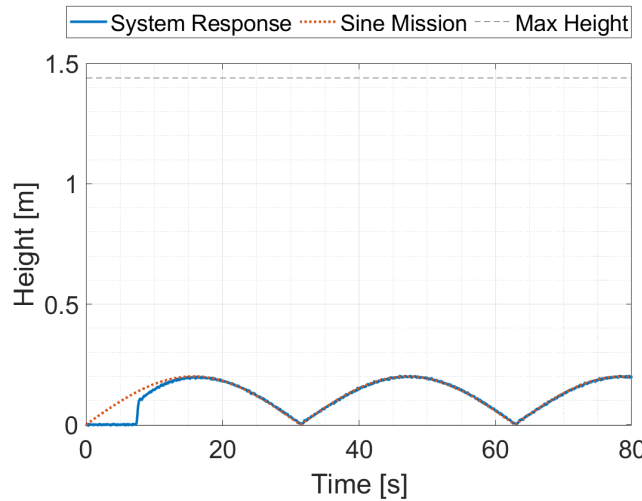


(a) Single PID Step Down

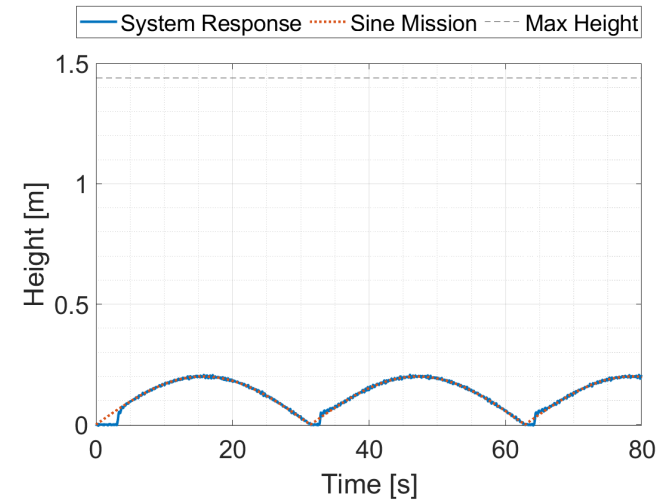


(b) Two PID Step Down

Figure 34: Step Down Mission Profiles with added noise

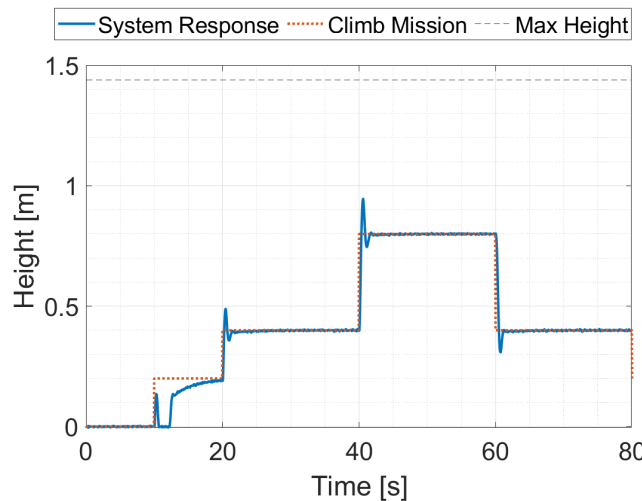


(a) Single PID Sine Mission

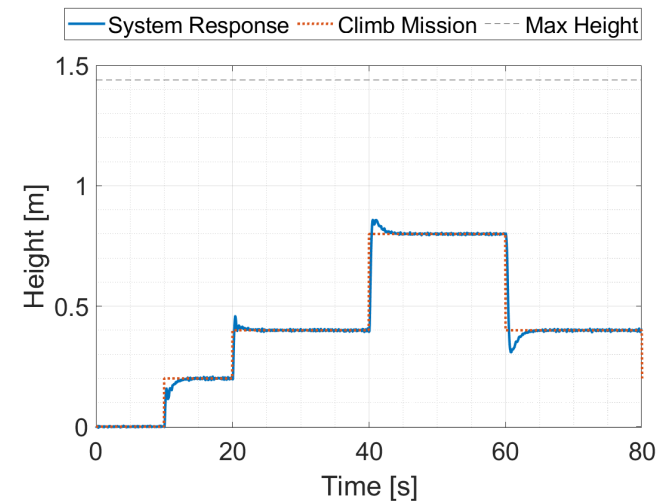


(b) Two PID Sine Mission

Figure 35: Sine Mission Profiles with added noise



(a) Single PID Climb Mission



(b) Two PID Climb Mission

Figure 36: Climb Mission Profiles with added noise